A prion accelerates proliferation at the expense of lifespan

David M. Garcia[1,2,+,*], Edgar A. Campbell[1,+], Christopher M. Jakobson[1], Mitsuhiro Tsuchiya[3], Acadia DiNardo[2], Matt Kaeberlein[3] and Daniel F. Jarosz[1,4,*]

[1]Department of Chemical & Systems Biology, Stanford University School of Medicine, Stanford, CA, 94305
[2]Institute of Molecular Biology, Department of Biology, University of Oregon, Eugene, OR, 97403
[3]Department of Pathology, University of Washington, Seattle , WA, 98195
[4]Department of Developmental Biology, Stanford University School of Medicine, Stanford, CA, 94305
[+]Equal contributions
*Corresponding authors: dmgarcia@uoregon.edu and jarosz@stanford.edu

ABSTRACT

Organisms often commit to one of two strategies: living fast and dying young or living slow and dying old. In fluctuating environments, however, switching between these two strategies could be advantageous. Lifespan is often inversely correlated with cell size and proliferation, which are both limited by protein synthesis. Here we report that a highly conserved RNA-modifying enzyme, the pseudouridine synthase Pus4/TruB, can act as a prion, endowing yeast with greater proliferation rates at the cost of a shortened lifespan. Cells harboring the prion can grow larger and exhibit altered protein synthesis. This epigenetic state, [*BIG*$^{+}$] (better in growth), allows cells to heritably yet reversibly alter their translational program, leading to the differential expression of hundreds of proteins, including many that regulate proliferation and aging. Our data reveal a functional role for aggregation of RNA-modifying enzymes in driving heritable epigenetic states that transform cell growth and survival.

Introduction

Cell size and proliferation are fundamental determinants of development, survival, and disease (Su and O'Farrell, 1998). Although these features can be independently controlled, coupling is common due to their dependence on the same biochemical building blocks (Su and O'Farrell, 1998; Turner et al., 2012). Growth and proliferation also impact lifespan across eukaryotes (Fontana et al., 2010; Kenyon, 2010; Pitt and Kaeberlein, 2015). The importance of tightly controlling each of these properties is underscored by the many mutations affecting growth and proliferation that are pathogenic, leading to cancer, developmental abnormalities, and myriad diseases of age (reviewed in (Hanahan and Weinberg, 2011; Saxton and Sabatini, 2017).

Organisms commonly alter the relationship between cell growth and proliferation during the course of development (Su and O'Farrell, 1998). In oocytes of *Drosophila melanogaster*, for example, a massive expansion in cytoplasmic volume without cellular division precedes a later step of numerous cellular divisions without cytoplasmic growth. The rates of cell growth and proliferation can be strongly coupled to nutrient sensing and to changes in metabolism (Efeyan et al., 2015; Turner et al., 2012). Thus, organisms can use genetically encoded signaling pathways to commit to different strategies depending on both their needs and their environment (Ivanov et al., 2015; Jung et al., 2018). Epigenetic tuning of cell growth and proliferation could in principle provide a stable yet reversible mechanism to alter the relationship between growth and proliferation according to differing needs in fluctuating environments. Histone modifications can enable such adaptation in a way that can be heritable over several

mitotic divisions. However, apart from a few notable exceptions (Catania et al., 2020; Grewal and Klar, 1996; Nakayama et al., 2000), the majority of studied examples are erased during meiosis (Heard and Martienssen, 2014; Moazed, 2011).

Prions are a distinct class of epigenetic mechanism that can be faithfully transmitted through both mitotic and meiotic cell divisions (Brown and Lindquist, 2009; Cox, 1965; Garcia and Jarosz, 2014; Wickner, 1994). The unusual folding landscape of prion proteins, which allows the recruitment of proteins from the naïve to the prion fold, promotes a mode of inheritance that is both stable and reversible (Chakrabortee et al., 2016a; McKinley et al., 1983). For example, transient perturbations in molecular chaperone activity (Brown and Lindquist, 2009; Chernoff et al., 1995), specific environmental stressors (Garcia et al., 2016; Singh et al., 1979; Tuite et al., 1981), or regulated proteolysis (Ali et al., 2014; Kabani et al., 2014) can induce or eliminate prion states. It is now appreciated that this form of information transfer is far more common than previously realized (Chakrabortee et al., 2016b; Halfmann et al., 2012; Yuan and Hochschild, 2017).

Here we investigate the inheritance of a prion-based epigenetic state that alters yeast cell physiology, potentiating a tradeoff between proliferation and lifespan. We first describe the [*BIG*$^{+}$] prion—driven by the conserved pseudouridine synthase Pus4 (known as TruB in mammals and bacteria)—which increases proliferation but shortens lifespan. We then quantitatively model the adaptive value of this *'live fast, die young'* growth strategy in fluctuating environments. [*BIG*$^{+}$] cells are larger and exhibit increased protein synthesis, as well as increased pseudouridylation activity. Finally, we find

72 evidence for analogous epigenetic control of cell size in wild yeast populations. The
73 epigenetic inheritance of an altered form of an RNA-modifying enzyme over long
74 biological timescales, as occurs in [*BIG*$^{+}$], thus provides a mechanism through which
75 short-lived epigenetic modifications of nucleic acid can be perpetuated across
76 generations.
77
78 **RESULTS**
79 **Cells bearing a prion-like epigenetic element live fast and die young**
80 We recently discovered more than 40 protein-based epigenetic elements in
81 *Saccharomyces cerevisiae* that are both heritable and reversible upon transient
82 perturbation of protein chaperone function (Chakrabortee et al., 2016a). Many of the
83 proteins that underlie this behavior have the potential to regulate growth. One of these
84 epigenetic states was induced by transient overexpression of the highly conserved
85 pseudouridine synthase *PUS4*/TRUB, which catalyzes formation of a ubiquitous
86 pseudouridine on U55 in tRNAs in bacteria, yeast and humans (Becker et al., 1997;
87 Gutgsell et al., 2000; Zucchini et al., 2003). Mutation of U55 leads to large fitness
88 deficits, second only to mutations in the tRNA anticodon loop, highlighting the functional
89 importance of this nucleotide (Li et al., 2016). Mutation of U55 is also linked to deafness
90 and diabetes in humans (Wang et al., 2016). We originally discovered this epigenetic
91 state because transient overexpression of *PUS4* led to an enduring and heritable
92 growth improvement in medium containing zinc sulfate (Chakrabortee et al., 2016a).
93 Upon closer examination, we noticed that cells harboring the Pus4-induced element

also achieved up to a ~60% faster maximal proliferation rate than naïve cells in standard rich medium (YPD; **Fig. 1A**, p=0.0095, unpaired t-test). We therefore initially named this mitotically heritable element "Big$^+$", for better in growth, on the basis of its phenotype.

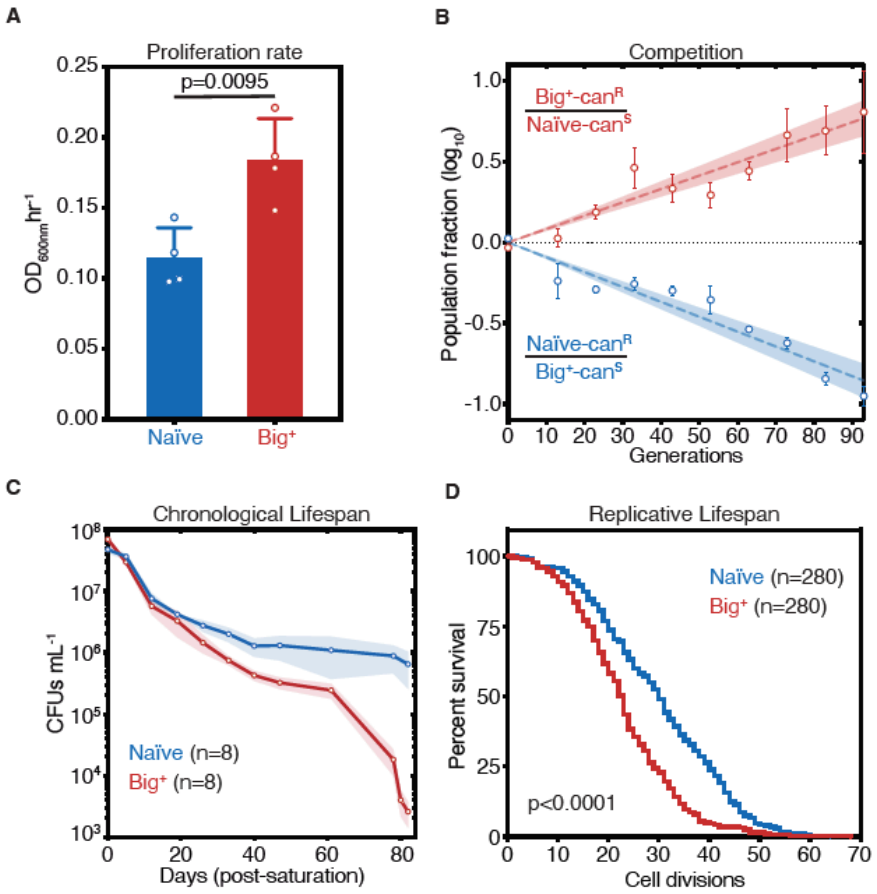

Figure 1. Cells bearing a prion-like epigenetic element live fast and die young.
(**A**) Big$^+$ cells proliferate faster than naïve cells. Bars represent mean of four replicates of maximum growth rate in YPD medium (measured by the peak of the derivative of the growth data), error bars are standard deviation, p=0.0095, unpaired t-test. (**B**) In a direct growth competition, Big$^+$ cells outcompete naïve cells. Raw data with standard error bars; trend line is dashed line showing shaded standard error; four replicates were performed for each competition. (**C**) Big$^+$ cells have a reduced chronological lifespan (CLS). Cells were grown to saturation in rich medium, and then transferred to nutrient poor medium and allowed to age for up to 80 days. Periodically samples were re-plated onto rich medium to measure remaining viability via colony forming units (CFUs). Thin lines are the average value from eight biological replicates with standard error represented by shading. (**D**) Big$^+$ cells have a reduced replicative lifespan (RLS). Starting with virgin mother cells, at each cell division daughter cells were separated and the total number yielded was counted for each replicate. n=280 per strain, combined from three independent experiments. P value < 0.0001, by Gehan-Breslow-Wilcoxon Test. Median survival: naïve=30 generations, Big$^+$=23 generations.

We next tested whether this growth advantage from the Big$^+$ epigenetic element would be more pronounced during direct competition and oscillating nutrient availability—as a single-celled organism such as yeast often face in nature. To do so, we performed a competition experiment that encompassed periods of abundant nutrient availability followed by starvation. Using resistance to canavanine as a marker for naïve and Big$^+$ strains, we mixed equal numbers of cells from each strain and propagated the mixed culture for close to 100 generations, diluting into fresh medium and measuring the fraction of the population that harbored the canavanine resistance marker every ~10 generations (**Supplementary Fig. 1A**). In these experiments, cells harboring Big$^+$ invariably outcompeted the genetically identical naïve cells that lacked it—they *live fast*—with a selection coefficient of nearly 1% (**Fig. 1B**). Competitions using reciprocally marked strains produced equivalent results. As a frame of reference, the fitness advantages that we measured for Big$^+$ are larger than those conferred by >30% of non-essential genes (Breslow et al., 2008) and the vast majority of natural genetic variants that have been quantified (Jakobson and Jarosz, 2019; Jakobson et al., 2019; Sharon et al., 2018; She and Jarosz, 2018).

Given the close link between proliferation and aging in many organisms (Bitto et al., 2015), we investigated whether Big$^+$ also influenced lifespan. Studies of aging in budding yeast have led to the discovery of numerous genes with conserved roles in aging of metazoans (Kaeberlein, 2010). These studies have measured two types of aging, both of which we tested here—chronological lifespan and replicative lifespan (Longo et al., 2012). Chronological lifespan is a measure of post-mitotic viability, during

which cells cease division under starvation conditions, until nutrients become available again. These conditions occur commonly in the natural ecology of this organism (Landry et al., 2006). To investigate, we aged cultures of naïve cells and genetically identical cells harboring Big$^+$ (**Supplementary Fig. 1B**). Over the course of 80 days, Big$^+$ cells had progressively lower viability than matched, isogenic, naïve controls (**Fig. 1C**).

Replicative lifespan is a measurement of the number of cell divisions that yeast can undergo before death (**Supplementary Fig. 1B**). These experiments revealed a significant difference in replicative potential between Big$^+$ and naïve cells—the median survival rate is reduced by seven generations (**Fig. 1D**, $p<0.0001$, Gehan-Breslow-Wilcoxon Test, and **Supplementary Fig. 1C**). This degree of lifespan shortening falls into the range seen for classic lifespan mutants: yeast lacking *SIR3* or *SIR4* have reductions of ~3–4 generations, and yeast lacking *SIR2* by ~10–11 generations (Kaeberlein et al., 2005; Kaeberlein et al., 1999). Thus, Big$^+$ cells harboring this Pus4-induced element exhibit both a significantly decreased chronological lifespan and replicative lifespan: they *die young*.

Modeling tradeoffs between proliferation and lifespan

We next investigated the adaptive value of the Big$^+$ phenotype by quantitatively modeling its fitness consequences in fluctuating environments, where committing to a single strategy can impose limits on the long-term fitness of a population. For example, when nutrient-rich periods tend to greatly exceed starvation periods, the rapid growth of the Big$^+$ phenotype might be favored, in spite of its die-young phenotype (**Fig. 2A**). But

this same decision could be maladaptive if growth conditions skewed towards frequent and longer periods of nutrient scarcity—where cells that grow slower and die older would instead have an advantage (**Fig. 2B**).

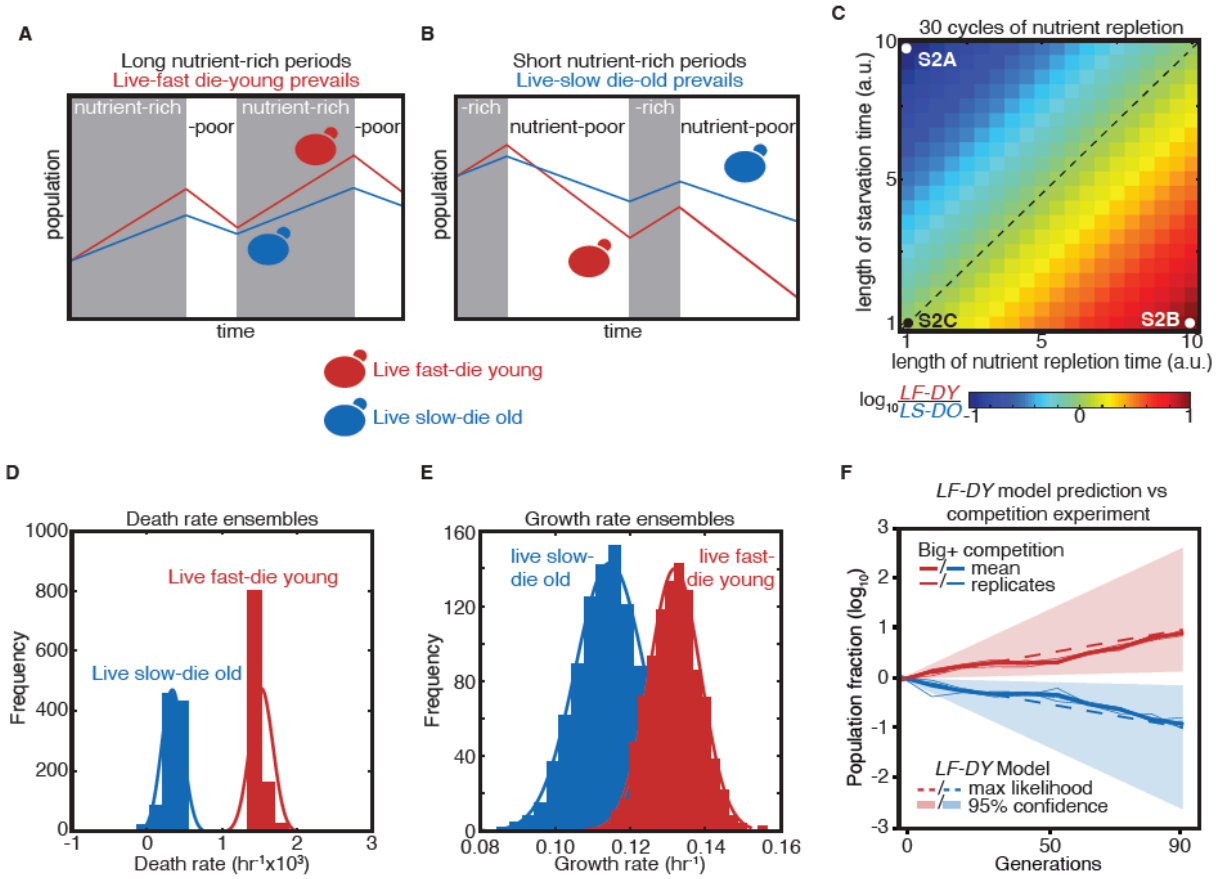

Figure 2. Modeling a reversible epigenetic live fast and die young strategy.
(**A**) A live fast–die young epigenetic element is beneficial for survival in environments with regular, extended nutrient-rich periods. (**B**) A live slow–die old growth state is beneficial for survival during conditions of repeated and extended starvation. (**C**) Simulated final population fraction (ratio of *LF-DY* to *LS-DO*) after 30 cycles of nutrient repletion and starvation, assuming a 1% growth advantage, a 1% higher death rate, and equal starting population sizes. Note log scale. (**D**) Monte Carlo sampling of exponential decay constant and (**E**) exponential growth constant distributions used to generate the ensemble of simulations shown in**,** (**F**) Monte Carlo simulation (dashed lines) of growth competition between *LF-DY* to *LS-DO* cells under parameters sampled from experimental growth and lifespan measurements of the Big$^+$ element (**Fig. 2D–E**). 95% confidence interval indicated by shaded areas. Shown in solid lines are the results of competitive growth between Big$^+$ and naïve cells as shown in **Fig. 1B** (mean: bold line; n = 4 biological replicates: thin lines).

To quantify these tradeoffs, we considered a population in which individuals heritably adopted one of these two strategies (live-fast-die-young, *LF-DY*, like Big$^+$ cells;

or live-slow-die-old, *LS-DO*, like naïve cells), modeling their fates in alternating nutrient environments (**Fig. 2C**). These simulations suggested that *LS-DO* cells should outcompete *LF-DY* cells when the periods of starvation are much longer than periods of nutrient abundance (**Supplementary Fig. 2A**). By contrast, *LF-DY* cells come to dominate the simulated culture when periods of nutrient abundance are much longer than periods of starvation (**Supplementary Fig. 2B**). When periods of starvation and nutrient repletion are of equal duration, both populations are equally fit (**Supplementary Fig. 2C**). When we varied the growth advantage and lifespan cost of the *LF-DY* sub-population, and also the periods of nutrient availability and starvation, we noted that each phase space contained regimes in which *either* strategy could be advantageous (**Fig. 2C** and **Supplementary Fig. 2D**).

Regimes in which either the *LF-DY* or *LS-DO* strategies would be strongly adaptive (and the other maladaptive) arose frequently under physiologically relevant environmental parameters. Oscillations within these regimes (i.e. between feast and famine) are common in nature (Broach, 2012), and withstanding them is essential for survival. Theory predicts that reversible epigenetic mechanisms, such as prions, could confer a selective advantage in fluctuating environments (King and Masel, 2007). Importantly, our model demonstrates that this advantage could derive not only from a tradeoff between improved stress resistance and impaired growth in normal conditions, but also from a growth advantage in times of plenty coupled with a disadvantage under stress.

196 Notably, the growth advantages we observed in our competition experiment were
197 quantitatively consistent with Monte Carlo simulations sampled from our experimental
198 measurements of the death rates (from chronological lifespan measurements, **Fig. 2D**)
199 and growth rates (from proliferation rate measurements, **Fig. 2E**) of individual cultures
200 in nutrient starved and replete conditions, respectively (**Supplementary Fig. 2E**). That
201 is, the adaptive advantages that we measured in competition were equivalent to those
202 that we predicted for a hypothetical *LF-DY* population after dozens of generations (**Fig.**
203 **2F)**. Thus, selection on these properties could be alone sufficient to favor maintenance
204 of the Big$^+$ state under the conditions we examined.
205
206 **Big$^+$ cells are large**
207 Positive correlations between growth rate and cell size have long been noted (Johnston
208 et al., 1977; Schaechter et al., 1958; Su and O'Farrell, 1998; Turner et al., 2012). To
209 determine if the faster-growing Big$^+$ cells were also larger, we examined them
210 microscopically, employing a widely-used image masking pipeline (Carpenter et al.,
211 2006). This allowed us to measure the sizes of thousands of cells from multiple
212 biological replicates, defining size distributions for both naïve and Big$^+$ populations.
213 During exponential growth, populations of Big$^+$ cells had a similar size distribution
214 to populations of naïve control cells. However, as the cultures became denser, naïve
215 control cells remained the same size whereas isogenic haploid Big$^+$ cells became larger
216 (**Fig. 3A** and **Supplementary Fig. 3)**. To simplify these comparisons, we scored
217 distributions by the fraction of very large cells that we observed (one standard deviation

or larger than the mean naïve size; **Fig. 3B**, n=4,678 and 5,501 cells shown for naïve and Big$^+$, respectively). This increase in mean area from 22.01 μm^2 to 25.36 μm^2 corresponds to a 23% larger volume (approximating the yeast cell as a sphere, naïve cell mean radius = 2.65 μm, Big$^+$ cell mean radius = 2.84 μm). In Big$^+$ cultures 33.1 $\pm$ (2.8)% of cells exceeded this threshold, whereas 16.5 $\pm$ (1.8)% did in naïve cultures (p=0.0011 by unpaired t-test; **Fig. 3C**).

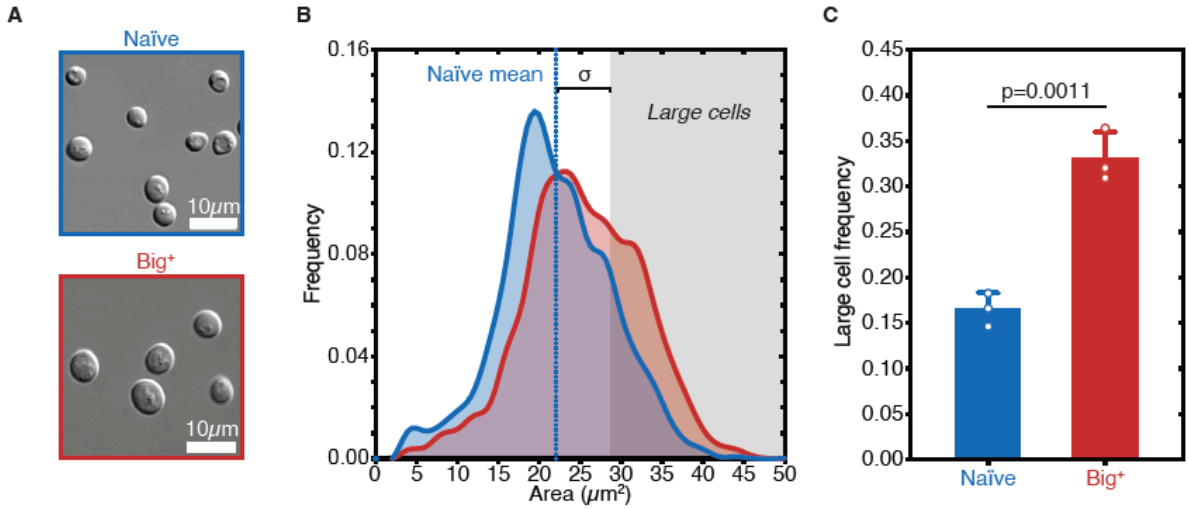

Figure 3. Big$^+$ cells are large.
(**A**) Micrographs of naïve and Big$^+$ haploid yeast cells. (**B**) Cell size distributions for thousands of naïve and Big$^+$ haploid cells (100% of distribution is shown, n=4,678 for naïve, n=5,501 for Big$^+$, dotted lines indicate mean). Large cell threshold begins at one standard deviation above the naïve mean. (**C**) The frequency of haploid cells above the large cell threshold. Bars represent mean of three replicate strains, for which thousands of cells are measured for each strain, error bars are standard deviation. p=0.0011, unpaired t-test.

[*BIG*$^+$] is a prion transmitted through mating and meiosis

Big$^+$ was originally induced by transient *PUS4* overexpression in a screen to identify prion-like epigenetic elements (Chakrabortee et al., 2016a). We therefore tested whether the increased cell size associated with this state was transmitted through genetic crosses with the unusual patterns of inheritance that characterize prion-based phenotypes (Brown and Lindquist, 2009; Cox, 1965; Wickner, 1994). We began by

239 mating the large haploid Big$^+$ cells to naïve haploids of the opposite mating type,
240 selecting diploid cells, and measuring their size. The resulting diploids were significantly
241 larger than those derived from control crosses with two naïve parents (**Fig. 4A–B**),
242 establishing that the trait is dominant.

243 We next investigated the meiotic inheritance of the large cell size trait. Because
244 they are not driven by changes in nucleic acid sequence, prions have unusual patterns
245 of inheritance that defy Mendel's laws. In addition to dominance in genetic crosses,
246 prion-based traits can be passed to *all* progeny of meiosis, in contrast to DNA-based
247 traits, which are inherited by half (**Supplementary Fig. 4A**)(Garcia and Jarosz, 2014; Li
248 and Kowal, 2012; Liebman and Chernoff, 2012; Wickner, 2016). We first mated control
249 naïve cells to naïve cells of the opposite mating type, sporulated the resulting diploids,
250 and dissected their meiotic progeny. We then grew clonal cultures of these haploid
251 meiotic progeny and examined their size distributions, which were indistinguishable
252 from their haploid naïve parents (**Fig. 4C**). In contrast, all cultures derived from the
253 meiotic progeny of Big$^+$ × naïve crosses were large (**Fig. 4C** and **Supplementary Fig.**
254 **4B**), a non-Mendelian pattern of inheritance that differs strongly from the expected
255 behavior for genetic mutants or chromatin-based epigenetic elements, but is consistent
256 with a prion-based mechanism of transmission. We therefore term this state "[*BIG*$^+$]"
257 (with capital letters indicating dominance and brackets denoting its non-Mendelian
258 pattern of segregation).

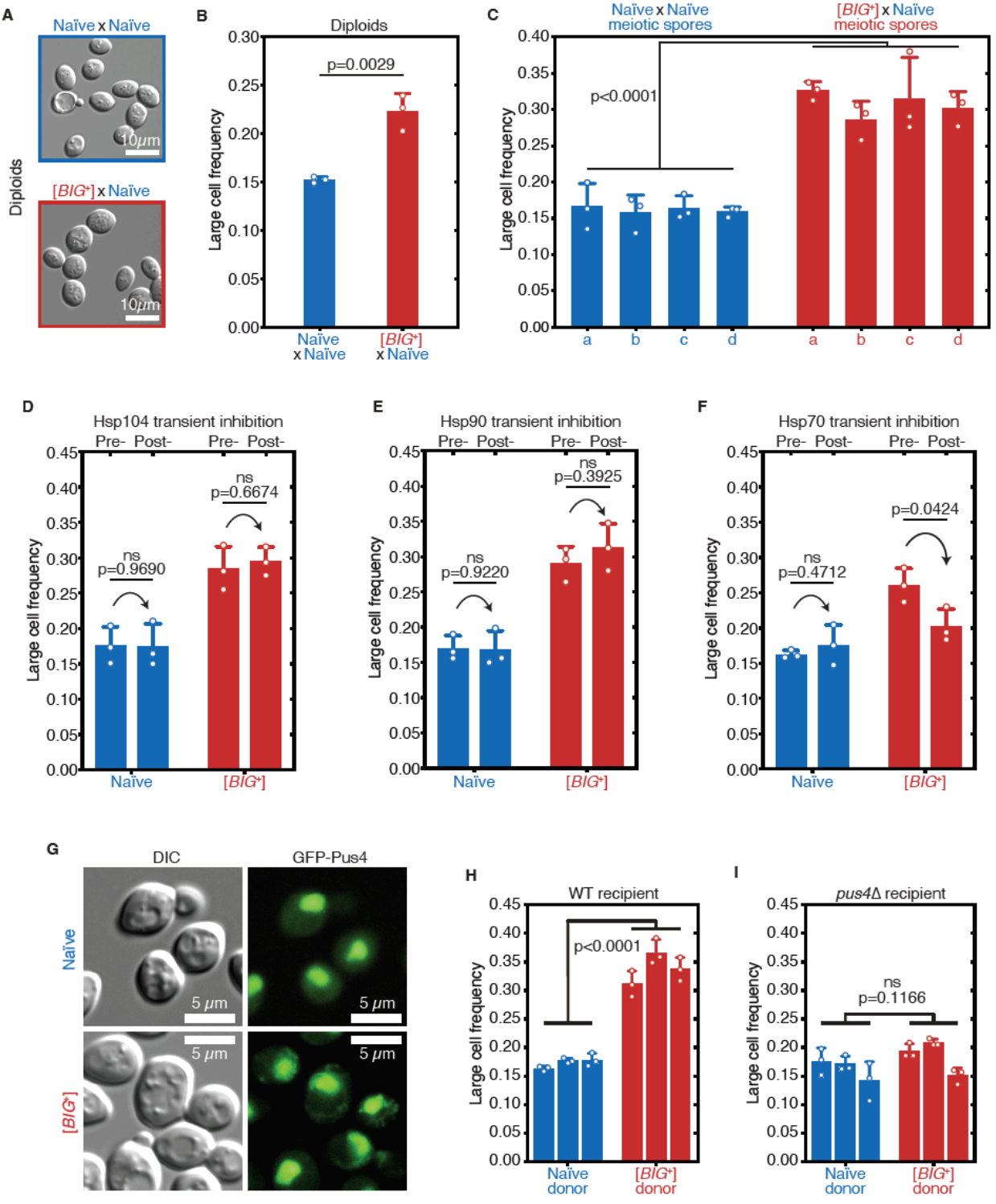

Figure 4. [*BIG*+] has prion-like patterns of inheritance.
(**A**) Micrographs of diploid yeast cells resulting from crosses of naïve and naïve parents, or naïve and [*BIG*+] parents. (**B**) The frequency of diploid cells above the large cell threshold. Bars represent mean of three replicate strains, for which thousands of cells are measured for each strain, error bars are standard deviation. p=0.0029, unpaired t-test. (**C**) Inheritance of large cell frequency to all meiotic spores. Bars represent the mean frequency of cells above the large cell threshold from three replicates, for which

thousands of cells were measured for each replicate, error bars are standard deviation. Difference between the means of four tetrad spores between naïve and [*BIG*$^+$], p<0.0001, unpaired t-test. (**D**) Transient inhibition of Hsp104 chaperone activity using guanidinium hydrochloride (GdnHCl) does not heritably alter the cell size trait. Bars represent the mean frequency of cells above the large cell threshold from three replicates, for which thousands of cells were measured for each replicate, error bars are standard deviation. Control samples (left bars of each pair) were propagated in parallel on nutrient-matched agar plates not containing GdnHCl. Post-inhibition represents strains subjected to GdnHCl treatment followed by recovery prior to cell size measurements (**Materials and Methods**). Naïve p=0.9690, [*BIG*$^+$] p=0.6674; unpaired t-test for both. (**E**) Transient inhibition of Hsp90 chaperone activity using Radicicol does not heritably alter the cell size trait. Bars represent the mean frequency of cells above the large cell threshold from three replicates, for which thousands of cells were measured for each replicate, error bars are standard deviation. Control samples (left bars of each pair) were propagated in parallel on nutrient-matched agar plates not containing Radicicol. Post-inhibition represents strains subjected to Radicicol treatment followed by recovery prior to cell size measurements (**Materials and Methods**). Naïve p=0.9220, [*BIG*$^+$] p=0.3925; unpaired t-test for both. (**F**) Transient inhibition of Hsp70 chaperone activity by expression of a dominant negative allele of *SSA1* permanently eliminates the [*BIG*$^+$] cell size trait. Bars represent the mean frequency of cells above the large cell threshold from three replicates, for which thousands of cells were measured for each replicate, error bars are standard deviation. Control samples (left bars of each pair) did not contain the *SSA1*^{K69M} constituitive expression plasmid but were propagated in parallel on non-dropout but otherwise nutrient-matched agar plates. Post-inhibition represents strains subjected to plasmid expression followed by plasmid removal and recovery prior to cell size measurements (**Materials and Methods**). Naïve p=0.4712, [*BIG*$^+$] p=0.0424; unpaired t-test for both. (**G**) The expression pattern of Pus4 is altered in [*BIG*$^+$] cells. (**H**) [*BIG*$^+$] can be transmitted via cytoduction into a wild-type recipient cell, consistent with a prion-based mechanism. Each bar represents the mean frequency of cells above the large cell threshold from three biological replicates, for which thousands of cells were measured for each replicate, error bars are standard deviation. Bars for three independent cytoductants are shown for each donor strain. Difference between the means of the three cytoductants between naïve and [*BIG*$^+$] donors: p<0.0001, unpaired t-test. (**I**) [*BIG*$^+$] is not transmitted via cytoduction into a *pus4*Δ recipient cell, indicating that prion transmission depends on continuous endogenous expression of Pus4. Each bar represents the mean frequency of cells above the large cell threshold from three biological replicates, for which thousands of cells were measured for each replicate, error bars are standard deviation. Bars for three independent cytoductants are shown for each donor strain. Difference between the means of the three cytoductants between naïve and [*BIG*$^+$] donors: p=0.1166, unpaired t-test.

[*BIG*$^+$] propagation requires the Hsp70 chaperone

The inheritance of prion-based phenotypes, in contrast to those driven by genetic mutations, is strongly dependent upon the protein homeostasis network (Garcia and Jarosz, 2014; Harvey et al., 2018; Liebman and Chernoff, 2012; Shorter and Lindquist, 2005). As a consequence, *transient* inhibition of molecular chaperones can lead to *permanent* elimination of prion-based traits. We therefore examined whether the large size of [*BIG*$^+$] cells also depended on protein chaperone activity (**Supplementary Fig. 4C**). Transient inhibition of the Hsp104 disaggregase, which regulates the inheritance of

many amyloid prions (Chernoff et al., 1995; Eaglestone et al., 2000; Halfmann et al., 2012; Shorter and Lindquist, 2004), had no effect on cell size in either naïve or [*BIG*$^{+}$] cells (**Fig. 4D**). Transient inhibition of the Hsp90 foldase, which regulates the transmission of a different subset of prions (Chakrabortee et al., 2016a), also had no impact on [*BIG*$^{+}$] transmission (**Fig. 4E**). By contrast, transient inhibition of Hsp70, via expression of a dominant negative *SSA1*^{K69M} allele (Chakrabortee et al., 2016a; Jarosz et al., 2014; Lagaudriere-Gesbert et al., 2002), caused [*BIG*$^{+}$] cells to permanently lose their large size phenotype (**Fig. 4F**). Thus like other prions (Brown and Lindquist, 2009; Chakrabortee et al., 2016a; Chakravarty et al., 2019), and unlike genetic mutations, propagation of [*BIG*$^{+}$] is dependent on the activity of this ubiquitous molecular chaperone.

We note that Hsp70 expression drops dramatically as yeast reach saturation and begin to starve (Werner-Washburne et al., 1989; Werner-Washburne and Craig, 1989), and also decreases as cells age (Janssens et al., 2015). These are two scenarios in which [*BIG*$^{+}$] is disadvantageous. Therefore, environmental conditions that favor growth, during which Hsp70 is abundant, also favor prion propagation. By contrast, conditions known to reduce Hsp70 expression and thereby increase prion elimination are also those in which prion loss would be favored.

Pus4 protein has a different expression pattern in [*BIG*$^{+}$] cells

Acquisition of [*PRION*$^{+}$] states often impacts the localization of the proteins that encode them. To visualize Pus4 expression in naïve and [*BIG*$^{+}$] cells, we employed a strain in

331 which an N-terminal GFP tag was appended at the endogenous *PUS4* locus (Weill et
332 al., 2018; Yofe et al., 2016). We did not observe large fluorescent foci typical of
333 canonical amyloid prions (Alberti et al., 2009). We did, however, observe altered
334 localization of Pus4. In naïve cells Pus4 consistently localized to the nucleolus, as has
335 been previously reported (Huh et al., 2003). In [*BIG*$^{+}$] cells the protein was also present
336 in the nucleolus. However, we also observed substantial fluorescence in a fragmented
337 network throughout the cytoplasm (**Fig. 4G)**, establishing that the distribution of Pus4
338 protein is altered in [*BIG*$^{+}$] cells. Although a high-resolution structure awaits
339 determination, our data are consistent with an altered physical state of Pus4 in [*BIG*$^{+}$]
340 cells.
341
342 **Endogenous Pus4 is required for propagation of [*BIG*$^{+}$]**
343 Although [*BIG*$^{+}$] was induced by a transient increase in Pus4, and was stable after
344 elimination of the inducing plasmid, we wanted to exclude the possibility that this prior
345 overexpression event might have established a positive feedback loop leading to an
346 enduring increase in Pus4 levels. We therefore constructed naïve and [*BIG*$^{+}$] strains
347 with a seamless N-terminal 3X-FLAG tag endogenously encoded at the *PUS4* locus.
348 Using immunoblots to detect the FLAG epitope in naïve and [*BIG*$^{+}$] cells, we observed
349 equivalent Pus4 levels, indicating that the phenotypes we observed in [*BIG*$^{+}$] cells were
350 not simply due to increased expression of this tRNA-modifying enzyme
351 (**Supplementary Fig. 4D**).

Prion proteins can be inherited through the cytoplasm and do not require exchange of genetic material for propagation. To test this, we performed a cytoduction, in which we mated [*BIG*$^{+}$] cells to naïve recipient cells of the opposite mating type carrying the *kar1-Δ15* mutation. Upon mating, this mutation prevents nuclear fusion, permitting mixing of cytoplasm, but not nuclei, between donor and recipient cells (**Supplementary Fig. 4E, Materials and Methods**) (Vallen et al., 1992). The transfer of [*BIG*$^{+}$] cytoplasm into naïve recipient cells resulted in the transfer of the [*BIG*$^{+}$] cell size phenotype (**Fig. 4H**). However, this was only the case for wild-type recipients. Naïve recipients lacking *PUS4* did not acquire the [*BIG*$^{+}$] cell size phenotype (**Fig. 4I)**.

It remained formally possible that a multi-protein prion state could be maintained by other cellular factors, even if prion-based phenotypes depended on Pus4. Therefore, we tested whether transient loss of *PUS4* was sufficient to permanently eliminate [*BIG*$^{+}$]. We first deleted *PUS4* from [*BIG*$^{+}$] and naïve cells. Upon *PUS4* deletion, the sizes of the mutants derived from naïve and [*BIG*$^{+}$] parents were equivalent (**Supplementary Fig. 4F**). Together with our cytoduction data, this suggested that continuous production of Pus4 is required to maintain this trait. Furthermore, *PUS4* deletion did not increase the size of naïve cells, suggesting that [*BIG*$^{+}$] does not inactivate Pus4, in contrast to many well characterized prions that phenocopy loss-of-function alleles of their underlying proteins (Byers and Jarosz, 2014). Finally, we restored the *PUS4* gene to its native locus in these same cells by homology-directed integration. Even after re-introduction of *PUS4*, the size distributions of both populations remained equivalent (**Supplementary**

373 **Fig. 4F**). Thus, both the expression and the propagation of the [*BIG*$^+$] phenotype require
374 the continual presence of a *PUS4* gene product.

375 These various lines of evidence—transmission to all meiotic progeny,
376 dependence on molecular chaperones, altered expression pattern, and requirement for
377 continuous expression of the protein that initiated the epigenetic trait—lead us to
378 propose that [*BIG*$^+$] is a protein-based element of inheritance, a prion, formed by the
379 Pus4 pseudouridine synthase.

380

381 **Pseudouridylation is maintained in [*BIG*$^+$] cells**

382 Because loss of *PUS4* did not phenocopy [*BIG*$^+$], but did block propagation of the prion,
383 we wondered whether the catalytic activity of Pus4 was maintained in [*BIG*$^+$] cells. To
384 measure pseudouridylation in naïve and [*BIG*$^+$] cells, we employed a qPCR-based
385 method that capitalizes on the enhanced susceptibility of pseudouridine to reacting with
386 CMC (1-cyclohexyl-(2-morpholinoethyl)carbodiimide metho-p-toluene sulfonate; **Fig.**
387 **5A**)(Lei and Yi, 2017). When pseudouridines are "labeled" by CMC, and these RNAs
388 are used as templates for replication by reverse transcriptase, the enzyme generates
389 nucleotide deletions and other mutations at these sites that can be detected by
390 differences in the melting temperature of the derived nucleic acid duplexes, compared
391 to non-pseudouridylated or unlabeled controls. Using this approach, we examined
392 pseudouridylation of an archetypical Pus4 substrate, $tRNA_{AGC}$ (Ala). When a
393 pseudouridine is present and CMC is added, the melting curve shifts relative to an
394 unlabeled control (no CMC). We observed a similar leftward shift in melting curves for

both naïve and [*BIG*$^+$] cells. In contrast, negative control cells missing the Pus4 protein, and therefore not pseudouridylated at U55, did not produce this shift (**Fig. 5B**). These data establish that Pus4-dependent modification of tRNAs is maintained in [*BIG*$^+$] cells.

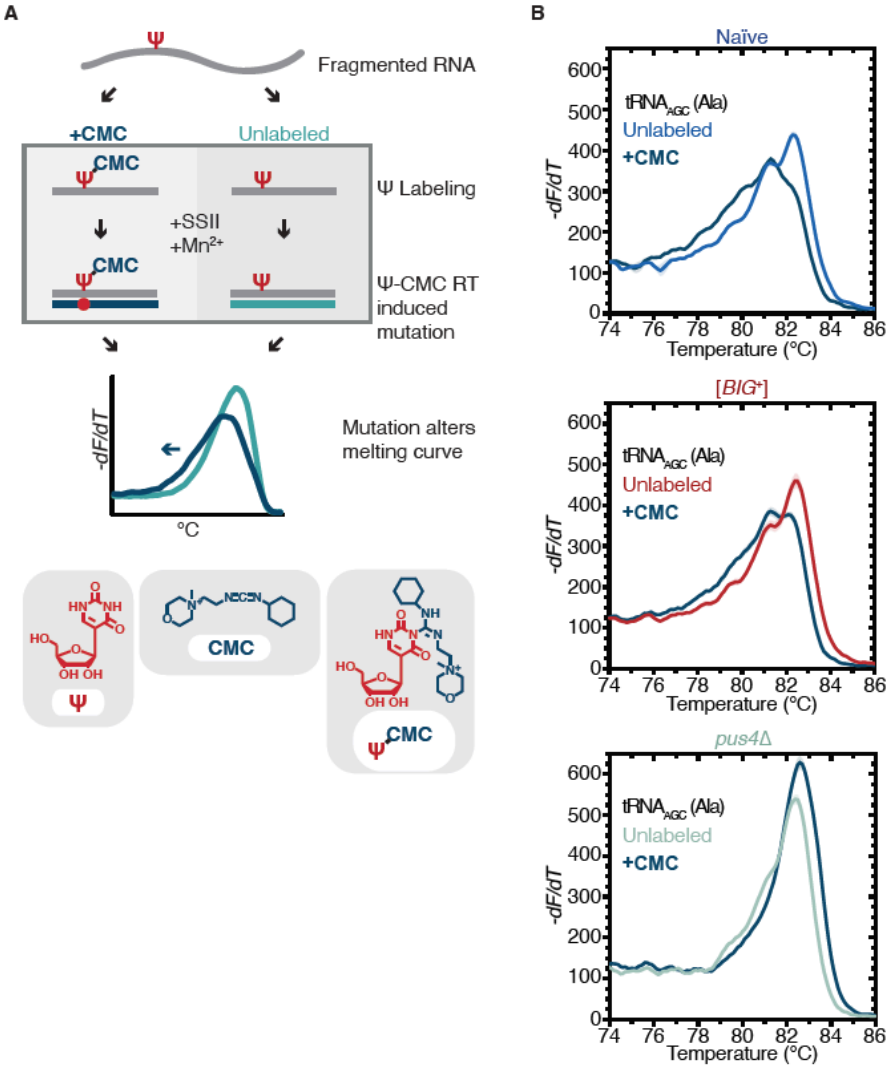

Figure 5. Pus4 activity is maintained in [*BIG*$^+$].
(**A**) Radiolabeling-free, qPCR-based method for locus-specific pseudouridine detection. Figure adapted from reference (Lei and Yi, 2017). (**B**) High resolution melting curve analysis demonstrates that Pus4-dependent pseudouridylation of $tRNA_{AGC}$ (Ala) is maintained in [*BIG*$^+$] cells but not in cells that do not contain Pus4p. Top panel: naïve samples CMC-labeled (black) or unlabeled (blue). Middle panel: [*BIG*$^+$] samples CMC-labeled (black) or unlabeled (red). Bottom panel: *pus4*Δ samples CMC-labeled (black) or unlabeled (torquoise). Solid lines representing melting curves are the mean of four replicates, with shaded areas representing standard error of the mean. The leftward shift of +CMC curves in naïve and [*BIG*$^+$] but not *pus4*Δ samples indicate Pus4-dependent pseudouridylation of U55.

Relative RNA levels are nearly unchanged in [*BIG*$^+$] cells

In addition to its ubiquitous pseudouridylation activity on all tRNAs, Pus4 also modifies some mRNAs (Carlile et al., 2014; Lovejoy et al., 2014; Schwartz et al., 2014). Some have posited that pseudouridylation impacts mRNA stability (Zhao et al., 2017). To discern whether the phenotypes of [*BIG*$^+$] cells might be due to relative changes in RNA levels, we performed RNA-sequencing. We grew naïve and [*BIG*$^+$] cultures in YPD medium until late exponential phase, extracted total RNA, and depleted it of rRNA. Comparing five replicates each of naïve and [*BIG*$^+$], the expression levels of only 15 genes changed significantly (thirteen decreased in expression and two increased, adjusted p-values < 0.1, Wald test, multiple testing correction with Benjamini Hochberg method), and these changes were modest (**Supplementary Table 2**). From this short list we did not observe any enrichments in gene ontology categories or pathway enrichments (YeastMine, *Saccharomyces* Genome Database (Cherry et al., 2012)). We conclude that the major effects of [*BIG*$^+$] during exponential growth (e.g. growth rate and replicative lifespan) do not occur via major changes to steady state mRNA levels.

To investigate whether the relative abundance of tRNAs is perturbed in [*BIG*$^+$] cells, we ran total RNA from naïve and [*BIG*$^+$] cells (grown to late-exponential phase) on a nucleic acid fragment analyzer, and quantified tRNA levels relative to a similarly abundant RNA that is not a target of Pus4, 5.8S rRNA (158nt)(**Supplementary Fig. 5**). We observed no significant differences. While we cannot exclude other effects on tRNA function or the relative abundance of particular tRNAs, our data show that bulk tRNA

abundance differences are likely also not responsible for the phenotypes of actively growing cells containing [*BIG*$^{+}$].

[*BIG*$^{+}$] cells are resistant to inhibition of protein synthesis

Because the increased cell size and proliferation, and reduced lifespan of [*BIG*$^{+}$] cells occur in the absence of major alterations to relative abundances of mRNA or tRNA, we wondered whether a change in protein synthesis might be responsible. To test this, we employed two inhibitors: 1) cycloheximide, an inhibitor of translational elongation (Baliga et al., 1969; McKeehan and Hardesty, 1969), and 2) rapamycin, a natural product macrolide that inhibits the TOR kinase, blocking a conserved signaling cascade that promotes protein synthesis (Beretta et al., 1996; Chung et al., 1992; Kuo et al., 1992; Price et al., 1992; Urban et al., 2007).

[*BIG*$^{+}$] cells grew nearly two-fold better than naïve cells in a sub-inhibitory concentration of cyclohexamide that was sufficient to impair proliferation (0.05 μg/mL; 100 μg/mL is used in experiments that rapidly and completely arrest translation) (**Fig. 6A**; compare to growth rates in **Fig. 1A**). [*BIG*$^{+}$] cells also proliferated faster in a concentration of rapamycin that inhibited growth (**Fig. 6B**), suggesting that the pathway may be more active in cells harboring the prion. This latter observation also provides a potential explanation for the decreased longevity of [*BIG*$^{+}$] cells: loss of TOR pathway function is associated with extended lifespan in yeast (Dikicioglu et al., 2018; Fabrizio et al., 2001; Powers et al., 2006) and many other organisms including nematodes, fruit flies, and mice (Bjedov et al., 2010; Harrison et al., 2009; Robida-Stubbs et al., 2012).

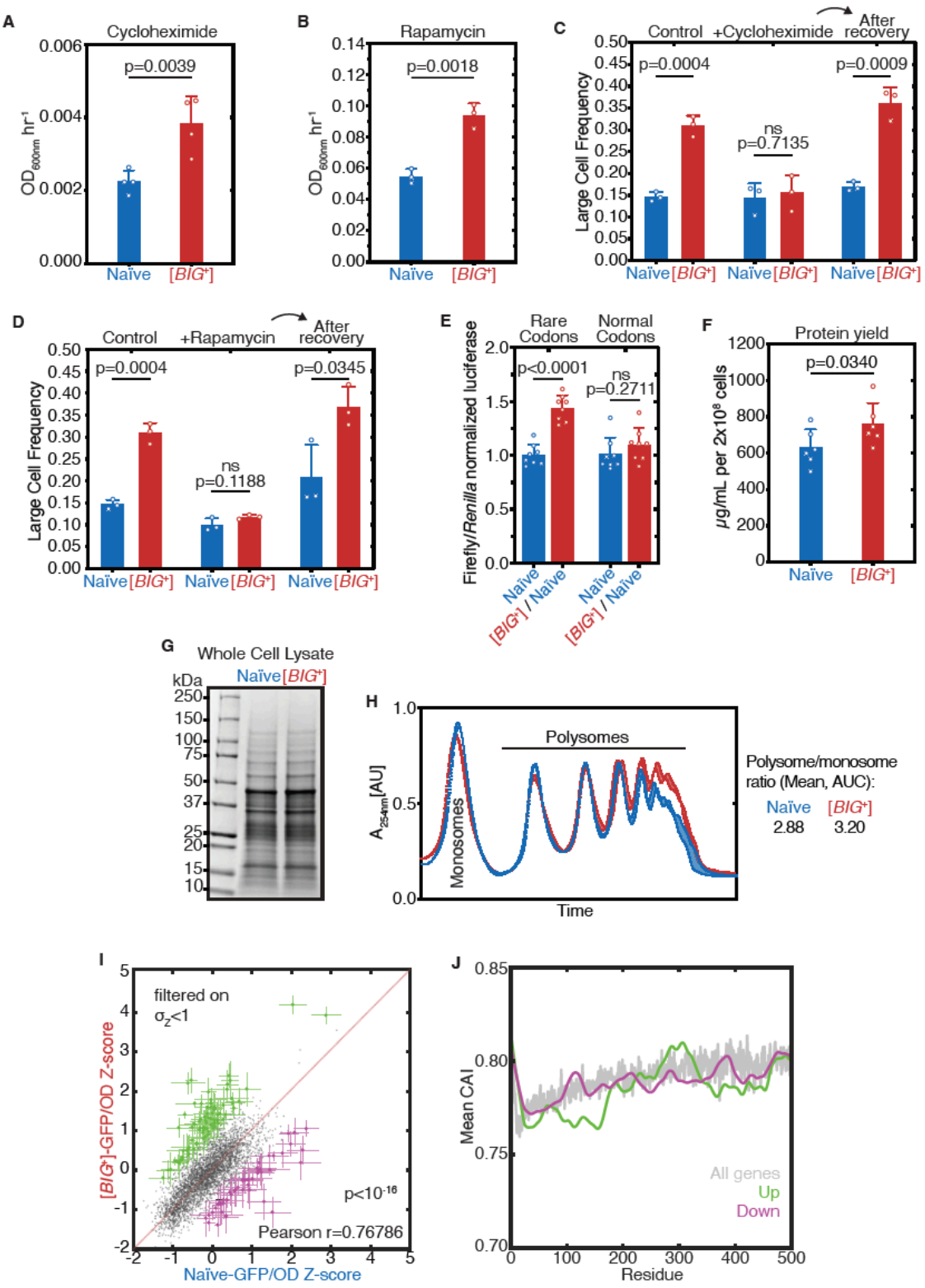

Figure 6. [*BIG*+] has altered protein synthesis.

(**A**) [*BIG*+] cells are resistant to translation elongation inhibitor cycloheximide. Bars represent the mean of the maximum growth rate in YPD+cycloheximide (measured by the peak of the derivative of the growth data) of four replicates, error bars are standard deviation, p=0.0039, unpaired t-test. (**B**) [*BIG*+] cells are resistant to TOR inhibitor rapamycin. Bars represent the mean of the maximum growth rate in

YPD+rapamycin (measured by the peak of the derivative of the growth data) of three replicates, error bars are standard deviation, p=0.0018, unpaired t-test. (**C**) [*BIG*$^+$] cells grown in cycloheximide are not larger than naïve cells. However after recovery they regain this phenotype. After treatment, cells were subcultured in YPD for ~75 generations before re-measuring the size in the absence of stress (see **Materials and Methods**). Bars represent the mean frequency of cells above the large cell threshold from three replicates, for which thousands of cells were measured for each replicate, error bars are standard deviation. Difference between the means of naïve and [*BIG*$^+$]: YPD control p=0.0004; YPD+cycloheximide p=0.7135; YPD after recovery p=0.0009; unpaired t-test for all. (**D**) [*BIG*$^+$] cells grown in rapamycin are not larger than naïve cells. However after recovery they regain this phenotype. After treatment, cells were subcultured in YPD for ~75 generations before re-measuring the size in the absence of stress (see **Materials and Methods**). Bars represent the mean frequency of cells above the large cell threshold from three replicates, for which thousands of cells were measured for each replicate, error bars are standard deviation. Difference between the means of naïve and [*BIG*$^+$]: YPD control p=0.0004 (same data presented in **Fig. 6C** as experiments were done in parallel); YPD+rapamycin p=0.1188; YPD after recovery p=0.0345; unpaired t-test for all. (**E**) [*BIG*$^+$] meiotic progeny translate more of a Firefly luciferase reporter containing rare codons than naïve meiotic progeny do. This effect is not seen in an mRNA variant that encodes an identical protein but contains codons more frequently used in yeast. Bars represent mean normalized luciferase values (an invariable *Renilla* luciferase gene is co-expressed from the same plasmid) from eight replicates: rare codons p<0.0001, normal codons p=0.2711, unpaired t-tests for both. (**F**) [*BIG*$^+$] cells produce more total protein per cell number than naïve cells, as measured by Bicinchoninic Acid (BCA) Assay. Bars represent the mean of six replicates, p=0.0340, unpaired t-test. (**G**) Coomassie stain of 15μg whole cell protein lysate from each strain suggests there are not major differences in the relative expression of the most abundant proteins in [*BIG*$^+$] cells compared to naïve cells. (**H**) [*BIG*$^+$] cells have more polysomes than naïve cells, as measured by polysome profiling. Lines for two technical replicates for each sample are shown, with the area between them shaded. Ratios (average of two technical replicates) were calculated by taking the lowest point between the monosome and disome peak as zero, and then calculating the ratios of the areas under the sum of the polysome peaks to that under the monosome peaks. (**I**) Plot showing proteome-wide GFP::protein fusion expression in [*BIG*$^+$] cells compared to naïve cells, highlighting ~130 proteins whose levels change. Each dot represents the mean of quadruplicate measurements of a single protein in naïve or [*BIG*$^+$] cells: black dots are proteins that did not change significantly as measured by Z-score change of less than 1.0 (σ_Z<1); green dots are protein fusions with higher fluorescence in [*BIG*$^+$] cells; violet dots are protein fusions with lower fluorescence in [*BIG*$^+$] cells. For colored dots, standard error of the mean is shown for both measurements from four biological replicates each. Pearson correlation of naïve and [*BIG*$^+$] cells, r=0.76786, and p<10^{-16} indicates that most proteins have correlated expression levels. OD_{600} was adjusted based on known blank wells, and the GFP/OD600 measurements were normalized by Z-score ($[x_i-\mu]/\sigma$) within the naïve and [*BIG*$^+$] populations independently. (**J**) Plot showing the protein residue number vs. the mean codon adaptation index (CAI) for all measured GFP-tagged proteins (grey line) and proteins whose levels were increased (green line) or decreased (violet line) in [*BIG*$^+$] relative to naïve cells in the proteome-wide screen. Proteins whose levels were elevated in [*BIG*$^+$] relative to naïve cells have a lower mean CAI in the 5´ ends of their mRNAs.

We next investigated whether these inhibitors impacted the size of [*BIG*$^+$] cells. When grown in cycloheximide or rapamycin to saturation, [*BIG*$^+$] cells were no longer large compared to naïve controls (**Fig. 6C–D**). Thus, unperturbed translation is necessary for the increased size of [*BIG*$^+$] cells. These data could be explained by the

inhibitors masking expression of the large cell trait, or by reversion of the [*BIG*$^+$] prion. To distinguish between these possibilities, we sub-cultured cells that had been treated with cycloheximide or rapamycin and allowed them to recover in rich medium for several dozen generations. We then examined their size distributions. Cell populations derived from [*BIG*$^+$] ancestors were once again significantly larger than naïve controls that we subjected to the same propagation regime (**Fig. 6C–D**). We conclude that [*BIG*$^+$] depends on protein synthesis to augment cell size, but that the prion is stable to transient perturbations in translation.

[*BIG*$^+$] increases protein synthesis

Translation is rate-limiting for growth in nutrient-rich conditions (Kafri et al., 2016). We observed enhanced growth of [*BIG*$^+$] cells in rich YPD medium (**Fig. 1A–B**). However, in synthetic defined medium with identical carbon source abundance (2% glucose), but fewer amino acids, nucleosides, and other nutrients for optimum growth (SD-CSM), [*BIG*$^+$] cells did not grow faster than naïve controls (**Supplementary Fig. 6A**) . These data, combined with the resistance of the prion cells to cycloheximide and rapamycin, suggested that protein synthesis might be enhanced in [*BIG*$^+$] cells.

Because a major component of translational regulation is the efficiency with which each mRNA is translated by the ribosome, we examined the impact of [*BIG*$^+$] on mRNAs encoded with different codons using luciferase reporter assays. We transformed [*BIG*$^+$] cells and isogenic naïve control cells with dual-luciferase plasmids encoding both *Renilla* and firefly luciferase genes. We tested two versions of the firefly

524 luciferase gene: the first contained the normal suite of firefly mRNA codons; the second
525 produced an identical protein product, but via codons that are more rare in *S.*
526 *cerevisiae*, reducing steady-state protein levels by ~five-fold (Chu et al., 2014). Each
527 plasmid also contained an internal control: the *Renilla* luciferase gene with its natural
528 set of codons. The firefly reporter with "normal" codons did not produce more luciferase
529 activity in [*BIG*$^{+}$] cells than in naïve cells, when normalized to the *Renilla* control (**Fig.**
530 **6E**). However, the firefly reporter with rarer codons produced normalized luciferase
531 levels approximately 50% higher in [*BIG*$^{+}$] cells than in isogenic naïve control cells (**Fig.**
532 **6E**). These data suggest that [*BIG*$^{+}$] cells may enhance translation of some proteins,
533 especially those containing a greater frequency of rare codons. We observed these
534 effects in both meiotic spores from naïve x [*BIG*$^{+}$] crosses (**Fig. 6E**), and the original
535 [*BIG*$^{+}$] isolates (**Supplementary Fig. 6B).** Therefore the altered translation phenotype,
536 like cell size, is inherited by all progeny of meiosis.

537 We next investigated whether [*BIG*$^{+}$] had global effects on the proteome by
538 isolating total protein from cells harboring the prion and naïve controls. We reproducibly
539 obtained more total protein per cell from the [*BIG*$^{+}$] cultures (**Fig. 6F**). We next loaded
540 an equal mass of protein lysate from naïve and [*BIG*$^{+}$] cells onto a denaturing
541 polyacrylamide gel and separated them by electrophoresis. Coomassie staining of these
542 gels showed no pronounced differences in banding patterns (**Fig. 6G**), suggesting that
543 [*BIG*$^{+}$] does not exert large changes on the composition of the major expressed portion
544 of the proteome, proteins which are known to be efficiently translated (Gingold and
545 Pilpel, 2011; Plotkin and Kudla, 2011).

We next performed polysome gradient analysis to assess global translation activity. We observed no change in monosomes or disomes in [*BIG*$^{+}$] samples compared to naïve controls. However, polysomes—which are responsible for most protein synthesis (Noll, 2008; Warner and Knopf, 2002)—were increased in [*BIG*$^{+}$] cells relative to naïve controls (**Fig. 6H**). In summary, we found that [*BIG*$^{+}$] cells have higher levels of translation, which increases total protein output, and may particularly increase the levels of some proteins translated from mRNAs enriched with codons that are more rare in yeast.

[*BIG*$^{+}$] reduces time spent in G1 phase of the cell cycle

Conditions that enhance protein synthesis also tend to reduce the fraction of time that cells spend in the G1 stage of the cell cycle (Jorgensen and Tyers, 2004). This is due to the fact that commitment to S phase entry—budding of a daughter yeast cell—depends on sufficient production of proteins needed to replicate the genome and essential cellular structures. Accelerating the production of these factors can thus shorten this period. We measured the fraction of naïve and [*BIG*$^{+}$] cells in the G1 phase of the cell cycle, by counting the fraction of unbudded cells (i.e. cells in G1). For naïve cells, 36.2% were in G1, whereas only 27.2% of [*BIG*$^{+}$] cells were in G1, a ~25% reduction (**Supplementary Fig. 6C,** p=0.0017, unpaired t-test). These data suggest that the cell cycle checkpoint for progression to S phase remains intact, and that a shortened G1 stage in [*BIG*$^{+}$] cells is consistent with their increased protein synthesis. [*BIG*$^{+}$] cells are not larger during exponential phase growth (**Supplementary Fig. 3**), suggesting that

568 their cell size checkpoint remains intact. Cells in stationary phase, by contrast, which do
569 not have the nutrient content needed to progress to S phase, may continue to
570 accumulate mass at a faster rate, contributing to their larger size.
571
572 **[*BIG*$^{+}$] cells enact an altered translational program**
573 Because relative mRNA expression levels were only subtly altered in [*BIG*$^{+}$] cells during
574 exponential growth phase, but multiple measures of translation were increased, we
575 considered the possibility that the phenotypes of the prion might be due to changes in
576 protein levels of particular open reading frames. To test this idea, we capitalized on the
577 dominance of [*BIG*$^{+}$] in genetic crosses (**Fig. 4B**), mating haploid cells harboring the
578 prion to a genome-wide collection of N-terminal seamless superfolder-GFP fusions
579 ("SWAT" library; ~5,500 ORFs; (Weill et al., 2018)). Equivalent matings between naïve
580 strains and this genome-wide collection served as controls. To control for the larger size
581 of the [*BIG*$^{+}$] cells, we assessed protein levels in these diploid strains in terms of the
582 relative GFP levels (normalized by OD_{600} and Z-scored) within the naïve and [*BIG*$^{+}$]
583 GFP-fusion collections separately. Mating and fluorescence measurements were
584 performed in biological duplicate: the SWAT library was mated to two separate [*BIG*$^{+}$]
585 isolates alongside naïve controls. The reported OD_{600}-normalized GFP levels are the
586 mean of two technical duplicates of each biological duplicate. Protein levels measured
587 in this way were generally well correlated between naïve and [*BIG*$^{+}$] strains (Pearson's r
588 = 0.76; $p < 10^{-16}$), in concordance with our results from electrophoresis of total cellular
589 protein. Yet many proteins were up- or down-regulated in [*BIG*$^{+}$] cells.

590 Of the 4,233 fusions whose abundance could be robustly quantified across the
591 four replicates ($\sigma_{Z\text{-score}} < 1$ for both naïve and [*BIG*$^+$]), ~130 were differentially expressed
592 in [*BIG*$^+$] cells. Consistent with a bias toward enhanced translation, 81 were upregulated
593 and 46 were downregulated (**Fig. 6I** and **Supplementary Table 3**). These proteins did
594 not show any strong enrichment in physiochemical properties (see **Supplementary**
595 **Text** for further discussion). Nor were they enriched in proteins encoded by the handful
596 of known Pus4-pseudouridylated mRNAs (Carlile et al., 2014; Lovejoy et al., 2014;
597 Schwartz et al., 2014). We also did not observe a widespread increase in expression of
598 ribosomal proteins. We did, however, observe that proteins that were increased in
599 [*BIG*$^+$] cells had a modest decrease in their codon adaptation index (CAI) at the 5´ end
600 of their mRNAs relative to all genes (**Fig. 6J**), indicating that cells harboring the prion
601 might more efficiently translate these messages. The dip in CAI that is typical in the 5´
602 end of all genes, known as “translational ramping”, is thought to reflect the bias toward
603 translational control near the beginning of ORFs (Frumkin et al., 2018; Tuller et al.,
604 2010). (Lower CAI can both reduce the speed of elongation by requiring rarer tRNAs
605 and lead to differences in mRNA structure that might also affect initiation or elongation
606 efficiency.) These data are consistent with our luciferase reporter data in which rarer
607 codons throughout the message output more protein in [*BIG*$^+$] than in naïve cells (**Fig.**
608 **6E** and **Supplementary Fig. 6B**), as well as the resistance of prion cells to the
609 elongation inhibitor cycloheximide (**Fig. 6A**).

610 Many hits were logically connected to the enhanced translation, increased size,
611 and shortened lifespan of [*BIG*$^+$] cells. The 81 upregulated proteins included multiple

612 ORFs whose deletions are associated with decreased cell size (such as *PHO5,*
613 *MRPS28, KAP122,* and *SWE1*) (Harvey and Kellogg, 2003; Jorgensen et al., 2002),
614 increased chronological lifespan (*DIG2* and *UBX6*) (Garay et al., 2014), and extended
615 replicative lifespan (*ENO1, MUB1, PHO87, PGM2,* and *YRO2*) (McCormick et al.,
616 2015). Conversely, the 46 downregulated proteins included ORFs whose deletions are
617 associated with increased cell size (*RNR4* and *RPL15B*) (Jorgensen et al., 2002;
618 Perlstein et al., 2005) and decreased chronological lifespan (including *BUD23*, *SMI1*,
619 *MHP1*, and *CLG1*) (Garay et al., 2014; Marek and Korona, 2013). Several proteins
620 directly involved in translation control and ribosome biogenesis were also increased in
621 [*BIG*$^{+}$] cells, including *FHL1, MRPS28, MRPS16, RPL24B, RPS7A, and UTP10*
622 (**Supplementary Fig. 6D**). The [*BIG*$^{+}$]-regulated proteins also included 29 ORFs
623 associated with differential sensitivity to rapamycin (including *SAS4, SNF1,* and *HCA4*)
624 (Butcher et al., 2006; Dudley et al., 2005; Kapitzky et al., 2010), and 14 ORFs that are
625 known genetic or physical interactors with TOR1 (including *GCD14* and *PAR32*)
626 (Krogan et al., 2006; Varlakhanova et al., 2018). The functional breadth of these effects
627 on the proteome, and their logical connection to factors involved in the control of
628 proliferation, cell size, and lifespan suggest that the phenotypes of [*BIG*$^{+}$] are likely
629 derived from an altered translational regulation program that favors growth and
630 proliferation at the expense of lifespan.
631
632 **Altered pseudouridylation in [*BIG*$^{+}$] cells**
633 Our finding that pseudouridylation on tRNA was maintained at similar levels in [*BIG*$^{+}$]

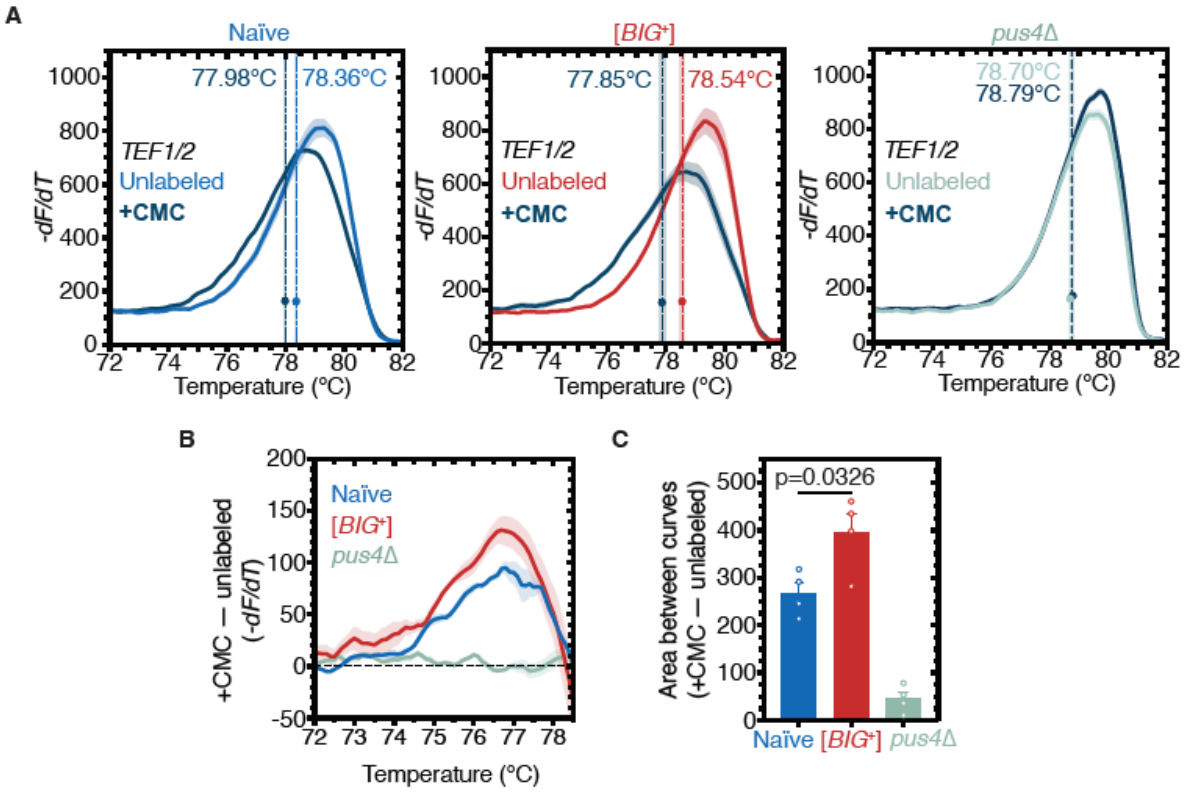

Figure 7. [*BIG*+] has elevated pseudouridylation.
(**A**) High-resolution melting curve analysis shows that U239 is pseudouridylated in *TEF1/TEF2* mRNA in both naïve and [*BIG*+] cells but not in cells that do not contain Pus4p. Left panel: naïve samples CMC-labeled (black) or unlabeled (blue). Middle panel: [*BIG*+] samples CMC-labeled (black) or unlabeled (red). Right panel: *pus4*Δ samples CMC-labeled (black) or unlabeled (turquoise). Dots mark the geometric center of four replicates, bisected by a dashed line with shaded area representing standard error of the mean. The melting temperature (Tm) of this point is also displayed. Solid lines representing melting curves are the mean of four replicates, with shaded areas representing standard error of the mean. (**B**) The difference in melting temperature behavior (*df/dT*) between CMC-labeled and CMC-unlabeled *TEF1/TEF2* mRNA amplicons is larger in [*BIG*+] cells than in naïve cells, suggesting higher levels of pseudouridylation of U239 in [*BIG*+] cells. Solid line represents mean of four replicates, with shaded areas showing standard error of the mean. (**C**) The difference in area between the melting curves of CMC-labeled and CMC-unlabeled *TEF1/TEF2* mRNA amplicons is greater in [*BIG*+] cells than in naïve cells, suggesting higher levels of pseudouridylation of U239 in [*BIG*+] cells. Bars represent the mean of four replicates, error bars indicate standard deviation, p=0.0326, unpaired t-test.

cells (**Fig. 5B**) led us to wonder whether mRNA substrates of Pus4 were similarly modified. The best-documented mRNA target of Pus4 is the translation elongation factor *TEF1/TEF2*—whose position U239 is robustly pseudouridylated in a Pus4-dependent manner (Carlile et al., 2014; Lovejoy et al., 2014; Schwartz et al., 2014).

These paralogous genes encode identical copies of the EF-1 alpha translation elongation factor, which binds to aminoacylated tRNAs—specifically the T arm stem-loop that is pseudouridylated by Pus4 (Dreher et al., 1999)—and delivers them to the A-site of the ribosome during translation elongation (Schirmaier and Philippsen, 1984). Using the aforementioned qPCR-based method for detecting pseudouridylation, we also found that *TEF1/TEF2* was pseudouridylated in our wild-type cells (both naïve and [*BIG*$^{+}$]), in a Pus4-dependent manner (**Fig. 7A**). Sanger sequencing verified that the modified position was identical to that previously annotated in the literature (**Supplementary Fig. 7A**).

The majority of studies on yeast prions have characterized them as decreasing or eliminating activity (Garcia and Jarosz, 2014). We recently discovered one notable exception, however, in which the [*SMAUG*$^{+}$] prion can increase the activity of the protein that encodes it (Vts1; (Chakravarty et al., 2019). We thus examined if there was an altered level of pseudouridylaton of *TEF1/TEF2* mRNA—if altered levels affected protein activity, this could be one possible mechanism linked to the altered translation program we found in [*BIG*$^{+}$] cells. By quantifying differences in the melt curve shift after CMC labeling—an analysis made simpler for *TEF1/TEF2* than for tRNAs by the absence of other pseudouridylated positions flanking U239—we observed an increase in the signal of pseudouridylation in [*BIG*$^{+}$] cells relative to naïve (**Fig. 7B–C** and **Supplementary Fig. 7B**). Together these data demonstrate that the catalytic function of Pus4 is retained in [*BIG*$^{+}$] cells, and can be enhanced for certain substrates, contrasting

with the classical view of prions as being loss-of-function protein conformations. They also provide a novel example of how RNA modification can be epigenetically controlled.

Epigenetic control of [*BIG*$^{+}$]-like phenotypes in wild yeast

Finally we tested whether protein-based epigenetic control of cell size, protein synthesis, or localization is present in wild yeast populations. Protein chaperones are

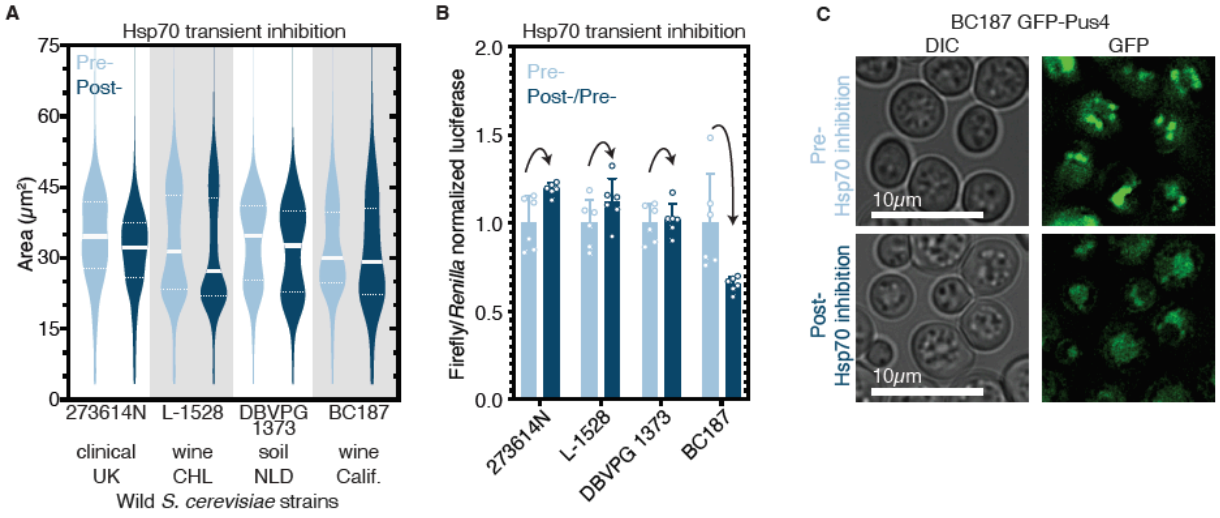

Figure 8. Epigenetic control of [*BIG*$^{+}$]-like phenotypes in wild yeasts.
(**A**) Transient inhibition of Hsp70 in diploid wild yeast strains from different niches around the globe leads to permanent reduction in cell size. Violin plots show all data from three biological replicates of each strain, light blue are cells before Hsp70 inhibition ("Pre-"), dark blue are cells after transient Hsp70 inhibition and recovery ("Post-"). Solid white line bisecting each distribution indicates mean; dotted lines indicate upper and lower quartiles. 273614N: clinical isolate from United Kingdom, Pre- vs. Post- $p<0.0001$. L-1528: wine isolate from Chile, Pre- vs. Post- $p<0.0001$. DBVPG 1373: soil isolate from the Netherlands, Pre- vs. Post- $p<0.0001$. BC187: wine isolate from California, Pre- vs. Post- $p<0.0001$. Kolmogorov-Smirnov test for all. (**B**) Transient inhibition of Hsp70 in wild yeast strains leads to permanent changes in protein synthesis capacity. Firefly reporter contains the "normal" suite of codons, which is normalized to internal control *Renilla* luciferase. Bars represent the mean of normalized luciferase values for six biological replicates, error bars are standard deviation. Light blue "Pre-" are cells prior to Hsp70 inhibition, dark blue "Post-" are cells after transient Hsp70 inhibition and recovery. A value above 1.0 for the dark blue bars indicates that the normalized translation capacity has increased after prion curing, a value below 1.0 indicates that capacity has decreased. 273614N $p=0.0134$, L-1528 $p=0.1397$, DBVPG 1373 $p=0.7428$, BC187 $p=0.0125$, unpaired t-test for all. (**C**) Transient inhibition of Hsp70 in BC187 wine isolate leads to permanent changes in Pus4p expression pattern, suggesting that its conformation may also be epigenetically regulated in wild strains. Prior to inhibition (top), cells show notable bright punctate structures; after transient inhibition and recovery (bottom), expression pattern becomes much more diffuse.

703 essential regulators of prion propagation in wild strains just as they are in laboratory
704 strains (Halfmann et al., 2012; Jarosz et al., 2014). To block the passage of prions in
705 wild yeasts, we transiently expressed a dominant negative variant (*SSA1*^{K69M}) of
706 Hsp70—the chaperone that is essential for [*BIG*$^{+}$] propagation (**Fig. 4F**)—in twenty wild
707 *S. cerevisiae* strains isolated from a variety of environments around the world (Cubillos
708 et al., 2009; Itakura et al., 2019). We measured the size of cells before and after this
709 chaperone curing and found four isolates—'273614N', (clinical, Newcastle, UK); 'L-
710 1528', (fermentation, Cauquenes, Chile); 'DBVPG1373', (soil, Netherlands); 'BC187',
711 (barrel fermentation, Napa Valley, California)—that became smaller after curing (**Fig.**
712 **8A**).

713 To test whether the four isolates that became smaller upon curing had altered
714 protein synthesis, we transformed them with the same luciferase reporters we tested in
715 laboratory [*BIG*$^{+}$] cells. We normalized the firefly reporters with variable codons to the
716 *Renilla* control for cured strains, and then normalized these to the corresponding
717 uncured strain values. Two of the four isolates showed significant changes to translation
718 (**Fig. 8B**). BC187 yielded the largest change upon curing, a ~40% reduction in
719 translation of a firefly containing a "normal" suite of codons, similar to what we had
720 observed with [*BIG*$^{+}$] cells generated in the laboratory.

721 We next examined the localization of Pus4 in BC187 and its Hsp70 'cured'
722 derivative. We transformed uncured and cured strains with a plasmid expressing GFP-
723 tagged Pus4 protein, and imaged cells using epifluorescence microscopy. In uncured
724 cells we observed distinct large puncta of Pus4. In contrast, in cured BC187 cells, the

725 signal was far more diffuse; few cells had large puncta compared to uncured cells (**Fig.**
726 **8C**).

727 These observations suggest that epigenetic, and potentially prion-mediated
728 control of mechanisms like the [*BIG*$^{+}$] prion that we have described here, may be
729 widespread in nature.

730

731 **DISCUSSION**

732 Epigenetic inheritance is most commonly thought to be driven by enzymes that modify
733 chromatin and DNA. Here we show that an enzyme that catalyzes epigenetic
734 modification of RNA can itself be controlled by an extrachromosomal epigenetic
735 process: a self-templating protein conformation that persists over long biological
736 timescales. This prion-based mechanism engages an altered translational program to
737 favor a '*live fast, die young*' strategy.

738 RNA modifications can facilitate multiple steps of protein synthesis, including
739 tRNA charging, ribosome biogenesis, and decoding (Sarin and Leidel, 2014). The
740 epigenetic conformational control of an ancient RNA modifying enzyme that we have
741 discovered provides a new translational control mechanism that strongly impacts
742 growth, proliferation, and lifespan. These data further define a type of 'recursive'
743 epigenetics, in which epigenetically transmissible information occurs via a protein that is
744 itself an epigenetic regulator—a protein that chemically modifies RNA. We found that
745 prion cells not only maintain pseudouridylation activity, but that activity can be
746 increased, even without a detectable increase in *PUS4* expression.

Although the protein that drives [*BIG*$^{+}$] modifies RNA, changes to relative RNA abundance do not appear to drive these growth or aging phenotypes. No major changes to relative tRNA or mRNA levels in actively growth cells are associated with [*BIG*$^{+}$]. Instead, changes to the translational control of numerous genes are logically connected to these phenotypes.

It is difficult to predict a priori how the increased level of pseudouridylation in *TEF1/TEF2* mRNA might impact the protein's activity. Due to a paucity of studies, the effects of pseudouridylation in ORFs is not well understood. Although the modification has been found to stabilize some mRNAs (Kariko et al., 2008; Nakamoto et al., 2017), recent evidence points to single sites slowing translation and altering decoding accuracy (Eyler et al., 2019). Given that our data are consistent with a change to translation elongation in [*BIG*$^{+}$] cells, and the major non-tRNA substrate of Pus4 is the *TEF1/TEF2* mRNA, encoding a central elongation factor that binds to and escorts tRNAs to the ribosome, future studies should address whether Pus4-dependent modification of *TEF1/TEF2* mRNA plays a role in the phenotypes of [*BIG*$^{+}$]. Apart from its pseudouridylation activity, the bacterial homolog of Pus4, *truB*, also harbors important tRNA chaperone activity (Keffer-Wilkes et al., 2016). It remains to be tested, however, if this activity is conserved in eukaryotic versions of the enzyme, and if so, what role if any that it plays in [*BIG*$^{+}$].

Translation is a rate-limiting step for growth in many organisms (Polymenis and Schmidt, 1997; Sonenberg, 1993) and is often activated in human cancers (Sonenberg and Hinnebusch, 2009). Other prions in yeast also affect translation, including [*PSI*$^{+}$]

769 and [*MOD*$^{+}$] (Baudin-Baillieu et al., 2014; Suzuki et al., 2012). However, in contrast to
770 [*BIG*$^{+}$], they lead to losses of their underlying protein activities, impairing translation and,
771 in turn, growth in many conditions (Baudin-Baillieu et al., 2014; Cox, 1965; Suzuki et al.,
772 2012). In contrast, in [*BIG*$^{+}$] cells, translation is amplified. This is also notable for the fact
773 that we have not found an example in the literature of a mutation that enhances
774 translation under nutrient replete conditions. Moreover, [*BIG*$^{+}$] did not require the
775 amyloid severing activity of Hsp104 that is critical for propagation of [*MOD*$^{+}$] and [*PSI*$^{+}$],
776 but rather the activity of a more generalist chaperone, Hsp70. A detailed description of
777 the molecular conformation of Pus4 protein in [*BIG*$^{+}$] cells, how it enables
778 pseudouridylation activity, and how it promotes translation are ripe questions for future
779 investigation.

780 Translation is also coupled to cell size, proliferation and lifespan (Ecker and
781 Schaechter, 1963; Kaeberlein and Kennedy, 2007; Lloyd, 2013; Steffen and Dillin,
782 2016; Tanenbaum et al., 2015). Cell size, which is determined in large part by activity of
783 the TOR pathway (Fingar et al., 2002; Zhang et al., 2000), has been inversely
784 correlated with lifespan (Anzi et al., 2018; He et al., 2014; Yang et al., 2011), and older
785 cells are larger (Egilmez et al., 1990). Moreover, molecules that extend lifespan, such
786 as rapamycin, also influence cell size and/or proliferation by restricting the cell's
787 translation capacity (Beretta et al., 1996; Terada et al., 1994). Here we describe an
788 epigenetic paradigm that links all of these fundamental cellular properties: translation,
789 cell size, proliferation, and lifespan. In future studies we would like to explore to what
790 extent the effect on lifespan may serve as material for selection to favor or disfavor

[*BIG*$^{+}$]. At present, we favor a hypothesis in which the aging defect of [*BIG*$^{+}$] cells is due at least in part to pleiotropic consequences of their increased proliferation and translation capacity. Although these features have already been linked to aging in genetic studies, we also note that such theories of antagonistic pleiotropy in aging are not without controversy (Hughes and Reynolds, 2005).

Replicative lifespan of wild budding yeast strains has been measured and varies widely (Kaya et al., 2015). Variation has been associated with changes in oxidative phosphorylation, respiration, and differences in metabolite biosynthesis. Genetic screening has also offered some insight as to the genetic basis of this variability (McCormick et al., 2015). Lastly, genetic mapping efforts have identified polymorphisms underlying natural chronological lifespan variation (Kwan et al., 2011). The genetic architecture of natural lifespan, both chronological and replicative, remains obscure, however. Our data further demonstrate that it can be subject to strong epigenetic control.

We note that prior studies have characterized genetic links between cell size and lifespan in yeast—mutants that make cells larger tend to age faster, and older cells tend to be larger than younger cells (Neurohr et al., 2019; Yang et al., 2011; Zadrag-Tecza et al., 2009). [*BIG*$^{+}$] provides an epigenetic mechanism to heritably alter these relationships. Exerting epigenetic, rather than genetic, control over basic cell growth behaviors could be valuable in the face of fluctuations between nutrient-replete and nutrient-poor conditions. Theory predicts that such mechanisms can have strong adaptive value when the frequency of fluctuations is rare relative to the generation time

of the organism (King and Masel, 2007). In agreement with these inferences, our modeling quantitatively described the long-run selective advantage of this '*live fast, die young*' prion state that we measured, illustrating the importance of considering not only steady-state phenotypes but also the ecological context in which prion states are expressed. Of particular relevance to this point is our data demonstrating that transient perturbation of Hsp70 activity can eliminate [*BIG*$^{+}$]. Conditions in which the prion confers a growth benefit match those that promote its propagation. Conversely, conditions in which the prion is detrimental, shortening lifespan, are also those known to reduce chaperone expression, and could thereby cure the prion. The strong dependence of [*BIG*$^{+}$] on chaperones therefore means that it is a natural epigenetic sensor of its environment.

Our data from wild yeast isolates demonstrates that cell size and protein synthesis are often under epigenetic control in nature. Exploring whether a [*BIG*$^{+}$]-like epigenetic mechanism that promotes proliferation in nutrient replete conditions is conserved in metazoans is a major goal for the future. Indeed cancer cells also experience frequent oscillations in their environments: as tumors grow and metastasize, cells are exposed to shifting gradients of oxygen and glucose that influence their growth rate (Martinez-Outschoorn et al., 2017; Schito and Semenza, 2016). Regulation of cell physiology in these situations is best understood at the level of transcriptional changes due to the relative ease of profiling them, but multiple lines of evidence suggest that translational hyperactivation can also fuel pathological proliferation (Robichaud et al., 2019). Our discovery of a protein-based mechanism that changes cell growth via

835 engagement of an altered translational program argues for greater investigation into the
836 epigenetic control of post-transcriptional processes, in both normal biology and disease.
837
838 **ACKNOWLEDGEMENTS**
839 We gratefully acknowledge Rebecca Freilich and Alan Itakura (Stanford University),
840 Mike Harms (University of Oregon), and Gabriel Neurohr (ETH Zürich) for their review of
841 the manuscript, and members of the Jarosz laboratory for helpful discussions. We thank
842 Maya Schuldiner (Weizmann Institute) for the generous gift of the SWAT GFP library.
843 We thank Kathrin Leppek and Maria Barna (Stanford University) for assistance with
844 polysome gradients and profiling and the use of their instrument. We thank Rebecca
845 Zabinsky and Thomas Lozanoski (Stanford University) for help with RNA-sequencing
846 analysis. We thank Adam Fries for assistance with microscopy and the Genomics and
847 Cell Characterization Core Facility for assistance with RNA quantification (Institute of
848 Molecular Biology, University of Oregon). DMG was supported by postdoctoral
849 fellowships from the NIH (F32-GM109680), Ford Foundation, and the Burroughs
850 Wellcome Fund Postdoctoral Enrichment Program (award number 1015119), in addition
851 to the University of Oregon, and a Pilot grant from the University of Washington Nathan
852 Shock Center (NIH P30AG013280). EAC was supported by an NSF Graduate Research
853 Fellowship. CMJ was supported by a postdoctoral fellowship from the NIH (F32-
854 GM125162). This work was also supported by grants to DFJ from the National Institutes
855 of Health (NIH-DP2-GM119140), the National Science Foundation (NSF-CAREER-
856 MCB116762), a Searle Scholar Award (14-SSP-210), a Kimmel Scholar Award (SFK-

15-154), and a Science and Engineering Fellowship from the David and Lucile Packard Foundation.

AUTHOR CONTRIBUTIONS

DMG, EC, and DFJ conceived and designed the project. DMG, EC, CMJ, MT and AD performed the experiments and analyzed data. CMJ implemented the modeling. MK supervised the replicative aging experiments. DMG, EC, CMJ, and DFJ wrote the manuscript. DFJ and DMG supervised the project.

COMPETING INTERESTS STATEMENT

The authors have no competing interests to declare.

Supplemental Figure 1

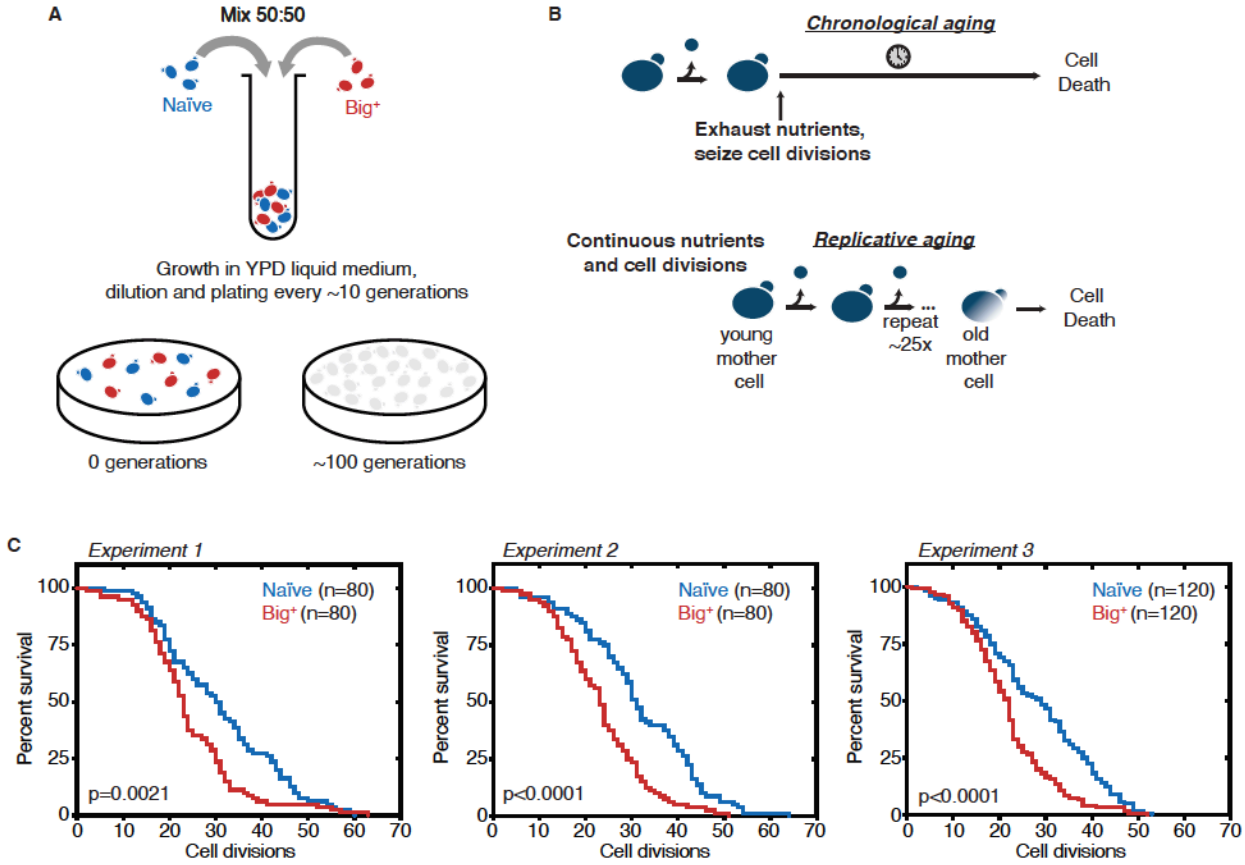

Supplementary Figure 1. Probing lifespan of Big⁺ cells.
(**A**) Experimental scheme for growth competition experiment associated with **Figure 1B**. (**B**) Experimental scheme for chronological and replicative lifespan measurements associated with **Figure 1C–D**. (**C**) Results from three independent RLS experiments, as combined into **Figure 1D**. Experiment 1: n=80 per strain, p value = 0.0021, by Gehan-Breslow-Wilcoxon Test. Median survival: naïve=30.5 generations, Big⁺=24 generations. Experiment 2: n=80 per strain, p value < 0.0001, by Gehan-Breslow-Wilcoxon Test. Median survival: naïve=31 generations, Big⁺=23 generations. Experiment 3: n=120 per strain, p value < 0.0001, by Gehan-Breslow-Wilcoxon Test. Median survival: naïve=29 generations, Big⁺=22 generations.

Supplemental Figure 2

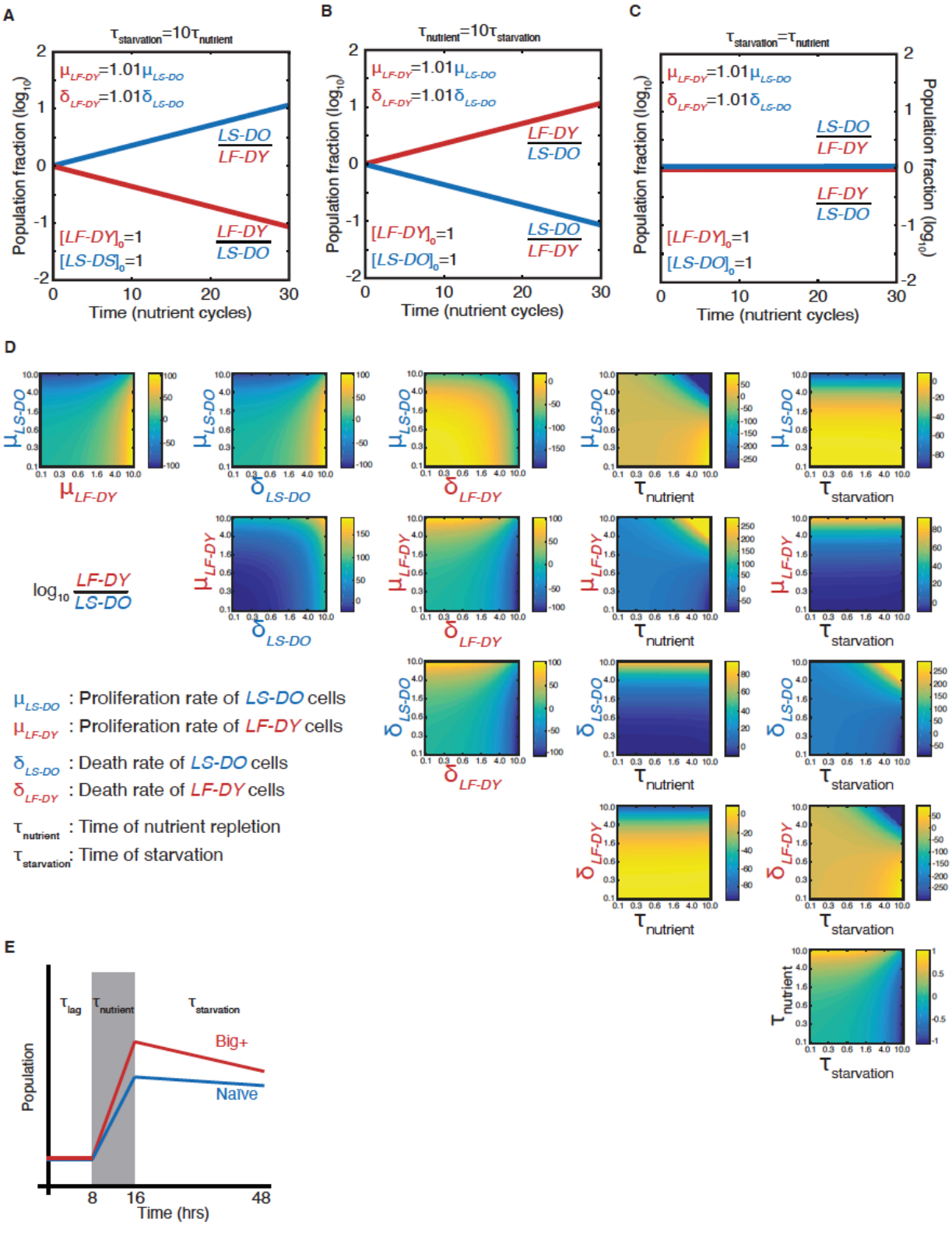

879

Supplementary Figure 2. Modeling a reversible epigenetic live fast and die young strategy.

Time-resolved simulations when (**A**) the period of starvation is ten times the period of nutrient repletion; (**B**) the period of nutrient repletion is ten times the period of starvation; and (**C**) the two nutrient regimes are of equal length. (**D**). Phase space representations of the simulated final population fraction (ratio of *LF-DY* to *LS-DO*) after 30 cycles of nutrient repletion and starvation, as in **Fig. 2C**. Indicated on the ordinate and abscissa of each panel are the parameters that were varied to generate each phase space. Parameters were varied over two orders of magnitude, as indicated. All other parameters were set to the baseline values as shown in **Supplementary Table 1**. (**E**) Schematic of parameters needed to model competitive growth experiment. During τ_{lag}, we assume that there is no change in population ratio. During $\tau_{nutrient}$, we require the exponential growth constants, and during $\tau_{starvation}$, we require the exponential decay constants (assuming cell death is a first-order process).

Supplemental Figure 3

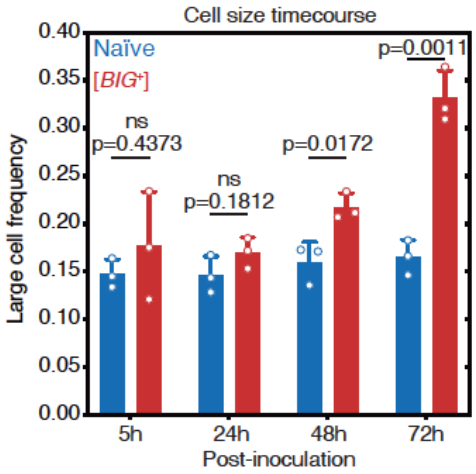

Supplementary Figure 3. The large cell phenotype of Big$^+$ emerges during the growth of a culture.

The large phenotype of Big$^+$ cells was stronger after three days of growth than after two days of growth (four days of growth yielded similar differences in cell size as for three days of growth, data not shown). The phenotype was not observed one day (24 hours) after inoculation or during the exponential growth phase (5 hours after inoculation). Bars represent the mean of three replicate strains—for which thousands of cells is measured for each—of the frequency of cells above the large cell threshold, error bars are standard deviation. Exponential growth (5 hours) p=0.4373, 24 hours p=0.1812, 48 hours p=0.0172, 72 hours p=0.0011; unpaired t-test for all.

Supplemental Figure 4

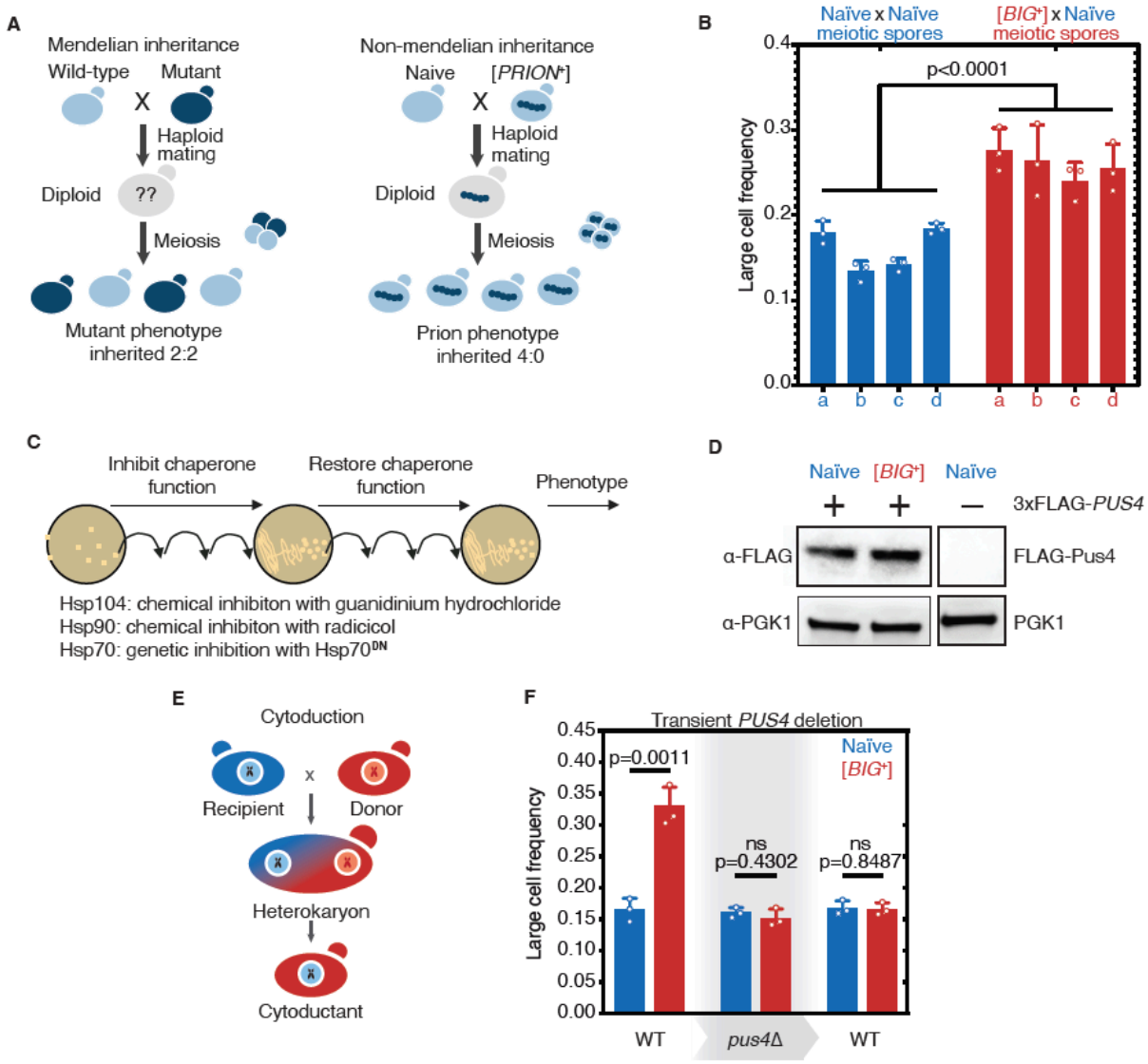

Supplementary Figure 4. Tests for prion-like patterns of inheritance and dependence on Pus4 for [*BIG*+].

(**A**) In contrast to mutations, which when arising from one parent are inherited in half of the meiotic progeny, prion-based traits can be inherited in all meiotic progeny. (**B**) Additional pairs of tetrads are shown for naïve and [*BIG*+] crosses. Bars represent the mean frequency of cells above the large cell threshold from three replicates, for which thousands of cells were measured for each replicate, error bars are standard deviation. Difference between the means of four tetrad spores between naïve and [*BIG*+], p<0.0001, unpaired t-test. (**C**) Experimental scheme carried out to test the roles of three different protein chaperones in the propagation of [*BIG*+]. Cells were exposed to various chaperone inhibitors, then propagated without inhibition to allow cells to recover, and then tested for retention of the large cell phenotype that existed prior to inhibition. (See **Materials and Methods**.) (**D**) Pus4p is expressed at similar levels in naïve and [*BIG*+]

cells. Naïve or [*BIG*$^{+}$] haploid cells were crossed to a strain containing a seamlessly N-terminally 3xFLAG-tagged *PUS4* gene, and total protein lysate was harvested, of which 15μg was loaded onto a PAGE gel for each sample, and then probed with anti-FLAG, or anti-PGK1 loading control antibodies. Negative control lane (untagged strain) is from the same blot. (**E**) Prion-based traits can be passed through cytoduction that exchanges cytoplasmic material without exchange of nuclear material. (**F**) Transient deletion of *PUS4* blocks inheritance of the large cell trait from [*BIG*$^{+}$] cells. Bars represent the mean frequency of cells above the large cell threshold from three replicates, for which thousands of cells were measured for each replicate, error bars are standard deviation. Differences between mean large cell frequencies of wild-type naïve and [*BIG*$^{+}$] cells prior to deletion, p=0.0011; after deletion of *PUS4*, p=0.4302; after re-introduction of *PUS4*, p=0.8487; unpaired t-test for all.

Supplemental Figure 5

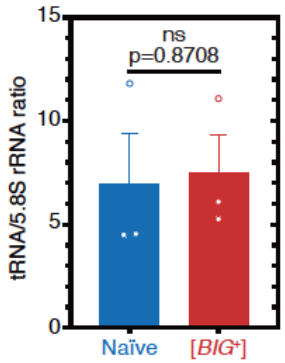

Supplementary Figure 5. Unchanged tRNA levels in [*BIG*$^{+}$].
tRNA levels are not different in [*BIG*$^{+}$] cells compared to naïve cells when normalized to non-Pus4 target 5.8S rRNA (158nt). Measurements represent the mean of three replicates with standard deviation shown, p=0.8708.

Supplemental Figure 6

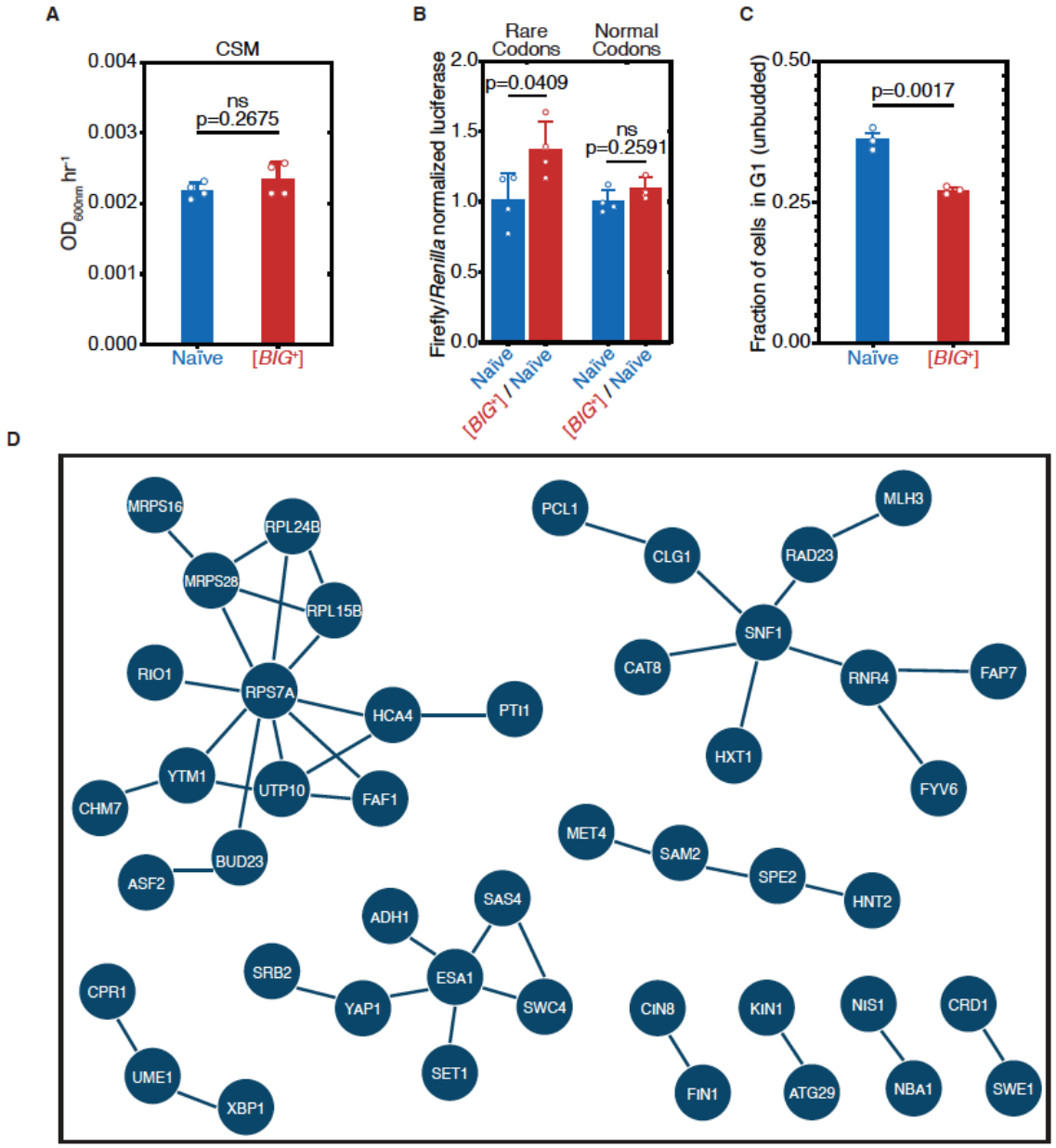

Supplementary Figure 6. Altered cell cycle and translation in [*BIG*$^+$]. (**A**) [*BIG*$^+$] cells do not exhibit enhanced proliferation in SD-CSM, a less nutrient-rich medium than YPD (**Fig. 1A**). Bars represent mean of four replicates of maximum growth rate (measured by the peak of the derivative of the growth data), error bars are standard deviation, p=0.2675, unpaired t-test. (**B**) Original [*BIG*$^+$] isolates translate more of a Firefly luciferase reporter containing rare codons than naïve cells do. This effect is not seen in an mRNA variant that encodes an identical protein but contains codons more frequently used in yeast. Bars represent mean normalized luciferase values (an invariable *Renilla* luciferase gene is co-expressed from the same plasmid) from four replicates: rare codons p=0.0409, normal codons p=0.2591, unpaired t-tests for both.

(**C**) The ratio of unbudded cells (G1 phase of the cell cycle) to budded cells (G2 and S phases) is reduced in [*BIG*$^{+}$]. Bars represent the mean of three replicates, error bars are standard deviation, p=0.0017, unpaired t-test. (**D**) Network representation of proteins whose levels change in [*BIG*$^{+}$] vs naïve cells in GFP fusion screen (**Fig. 6I** and **Supplementary Table 3**), generated from STRING (string-db.org). Solid lines link proteins with genetic and/or physical interactions. The largest cluster—upper left—contains proteins involved in ribosome assembly and translation.

Supplemental Figure 7

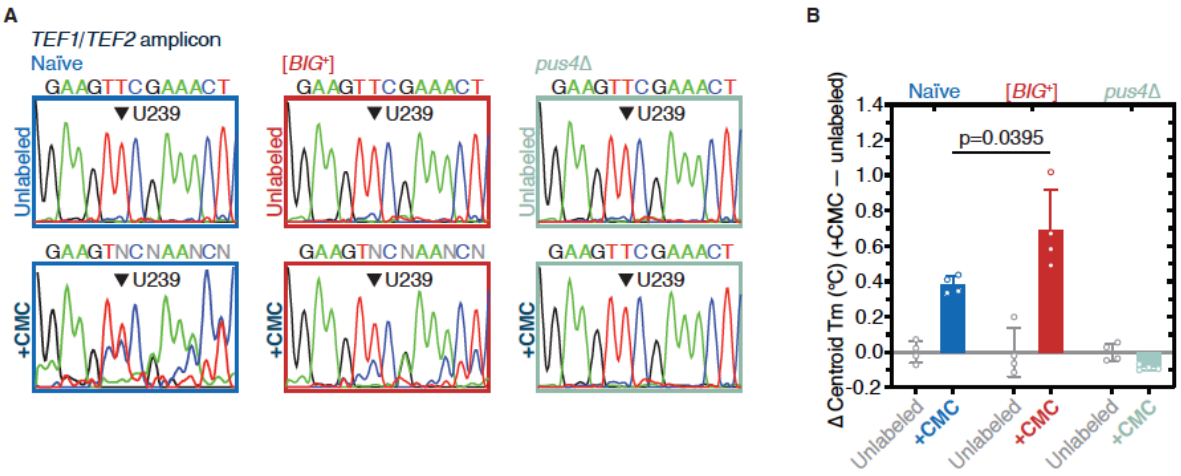

Supplementary Figure 7. [*BIG*$^+$] has elevated pseudouridylation.
(**A**) Sanger sequencing profiles from control and CMC-labeled RNA from naïve, [*BIG*$^+$], and *pus4*Δ cells. Naïve and [*BIG*$^+$] samples show characteristic mixed nucleotide assignments at previously annotated pseudouridylated position U239 in *TEF1/TEF2* mRNA, as well as more variable assignments 3´ or this position, indicating the presence of a mixed population of amplicons containing CMC-pseudouridine induced mutations and deletions. (**B**) The difference in Tm between the curves of CMC-labeled and CMC-unlabeled *TEF1/TEF2* mRNA amplicons is greater in [*BIG*$^+$] cells than in naïve cells, suggesting higher levels of pseudouridylation of U239 in [*BIG*$^+$] cells. Each bar represents the mean of four technical replicates of the change in the centroid Tm, or the center of the distribution in both the x and y dimensions. Error bars are standard deviation. Difference between naïve and [*BIG*$^+$], p=0.0395, unpaired t-test.

Supplementary Table 1: Parameter values used for the competitive fitness models shown in Figure 2 and Supplementary Figure 2.

Parameter	Meaning	Value
x_0	number of *LS-DO* cells	n/a
x_1	number of *LF-DY* cells	n/a
x_{00}	Initial number of *LS-DO* cells	1
x_{10}	Initial number of *LS-DO* cells	1
μ_0	Growth rate of *LS-DO* cells	1
μ_1	Growth rate of *LF-DY* cells	1.01
δ_0	Death rate of *LS-DO* cells	1
δ_1	Death rate of *LS-DO* cells	1.01
τ_1	Time of nutrient repletion	1
τ_2	Time of starvation	1

Supplementary Table 2: RNA-sequencing results

See .xls file for TPMs for each gene in five replicates of naïve and five replicates of [*BIG*$^+$]. Genes that showed significant differences are listed in a separate tab.

Supplementary Table 3. Proteins whose expression is changed in [*BIG*$^+$] cells.

See .xls file

Supplementary Table 4. Yeast strains, plasmids and oligonucleotides used in this study. See .xls file

985 **Supplementary Text**

986 We also examined the relationship between the proteins whose expression was altered
987 in [*BIG*$^{+}$] cells and other features related to gene expression, including mRNA
988 secondary structure and pseudouridylation. Comparing the altered gene set to yeast
989 transcripts with more double-stranded regions (Kertesz et al., 2010), no relationship
990 emerged. We also compared the gene list to mRNAs that are pseudouridylated by Pus4
991 (Carlile et al., 2014; Lovejoy et al., 2014; Schwartz et al., 2014), but did not see any
992 significant correlation or changes among the limited number targets that contained
993 Pus4-dependent pseudouridylation sites in both studies, and which were present in the
994 SWAT gene collection (thirteen genes total). We conclude that the changes we observe
995 for the translation of ~130 messages cannot be explained by Pus4-dependent
996 pseudouridylation of their mRNAs. Given the limited reproducibility of mapping
997 pseudouridylation sites transcriptome-wide in yeast from past studies, with large
998 variability sample to sample (Safra et al., 2017; Zaringhalam and Papavasiliou, 2016),
999 higher precision measurements in the future may offer the opportunity to compare anew
1000 those mRNAs pseudouridylated by Pus4 and their protein levels in [*BIG*$^{+}$] vs naïve cells.

1001 We also did not observe any relationship between genes with increased or
1002 decreased protein levels in [*BIG*$^{+}$] and isoelectric point (pI), protein length, protein half-
1003 life, or GO category enrichments (process, component or function). We did however
1004 observe several properties that were altered in both the genes that went up and those
1005 that went down: hydropathy score (GRAVY)(Kyte and Doolittle, 1982), aromaticity, and
1006 codon adaptability index (CAI), codon bias, and frequency of optimal codons. We

observed some amino acid enrichments as well, with genes going up in [*BIG*$^{+}$] being depleted in leucine, phenylalanine, and proline, and those down depleted in phenylalanine and aspartic acid.

Finally, given that many of the effects that we measured were post-transcriptional, we also examined genes with altered GFP levels (significantly up or down) in [*BIG*$^{+}$] cells using the MEME Suite, specifically for enrichment of predicted binding sites for RNA binding proteins (Bailey et al., 2009). We found that binding sites for the CCR4-NOT deadenylase complex were significantly enriched in our hits (motif alt ID CNOT4; consensus motif ACACAWA; adjusted p-value 0.0135).

MATERIALS AND METHODS

Model formulation.

To model the fitness of an epigenetic element for which growth in nutrient-replete conditions is improved and survival in starvation conditions is worsened, we define the following growth equations in nutrient-replete conditions:

$$x_0 = x_{00}e^{\mu_0 t}$$

$$x_1 = x_{10}e^{\mu_1 t}$$

Where x_0 represents the population of naive cells and x_1 represents the population of [*BIG*$^+$] cells. μ_0 and μ_1 are the growth rates of naive and [*BIG*$^+$] cells, respectively. We neglect the lag and stationary phases of growth, as the ratio between populations does not change during this time.

Likewise, in starvation,

$$x_0 = x_{00}e^{-\delta_0 t}$$

$$x_1 = x_{10}e^{-\delta_1 t}$$

Where δ_0 and δ_1 are the death rates of naive and [*BIG*$^+$] cells, respectively.

We can furthermore define the times of nutrient repletion and starvation as τ_1 and τ_2, respectively. Thus, for each cycle of nutrient/starvation, we can define the following recursion relations:

$$x_{0,i+1} = x_{0,i}e^{\mu_0\tau_1}$$

$$x_{1,i+1} = x_{1,i}e^{\mu_1\tau_1}$$

$$x_{0,i+2} = x_{0,i+1}e^{-\delta_0\tau_2}$$

$$x_{1,i+2} = x_{1,i+1}e^{-\delta_1\tau_2}$$

And we can write an analytical expression for the ratio of populations after one repletion/starvation cycle:

$$x_0(t+\tau_1+\tau_2) = x_0(t)e^{\mu_0\tau_1-\delta_0\tau_2}$$

$$x_1(t+\tau_1+\tau_2) = x_1(t)e^{\mu_1\tau_1-\delta_1\tau_2}$$

$$\frac{x_1}{x_0}(t+\tau_1+\tau_2) = \frac{x_1(t)}{x_0(t)}e^{(\mu_1\tau_1-\delta_1\tau_2)-(\mu_0\tau_1-\delta_0\tau_2)}$$

For the purposes of the model, we consider only the ratio between populations in the two epigenetic states (neglecting the total carrying capacity of the environment). The above defines a recursion relation from which we can predict the ratio of naive and [*BIG*$^+$] cells after N cycles of nutrient repletion and starvation.

Parameter estimation and prediction of competitive fitness. The free parameters defining the growth advantage and starvation disadvantage attributable to the

epigenetic element in the model above (μ_0 and μ_1; δ_0 and δ_1) were determined by Monte Carlo sampling of independent measurements of the growth and death rates (**Fig. 2D–E**). To generate the ensemble of competitive fitness predictions shown in **Figure 2C**, we randomly sampled growth and death rates for naive and [*BIG*$^+$] cells according to their experimentally determined distributions. The sampling was conducted 1000 times, and the prediction shown in **Figure 2F** is the median and 95% confidence interval of the resulting ensemble of model predictions.

Code and data availability. All MATLAB code and data required to generate the model predictions is available at github.com/cjakobson/liveFastDieYoung. Code to generate the figures is available upon reasonable request to jarosz@stanford.edu.

Bacterial strain growth. Bacteria strains (for plasmid propagation) were cultured on LB agar or liquid (Research Products International (RPI), Mount Prospect, IL).

Yeast strains. Yeast strains were cultured on either YPD agar or liquid (RPI) or SD-Ura (Sunrise Scientific, Knoxville, TN), unless otherwise indicated. Strains were stored as glycerol stocks (25% glycerol (Amersco, Solon, OH) in appropriate media) at -80 °C and revived on YPD or amino acid dropout media before testing. Yeast were grown in YPD at 30 °C on a TC-7 roller drum wheel (New Brunswick) unless indicated otherwise. Yeast transformations were performed with a standard lithium–acetate protocol (Gietz et

al., 1992). The *pus4*Δ strain was sourced from the BY4741 MATa haploid knockout library (GE Dharmacon, Lafayette, CO).

Strain constructions. Most diploids were constructed by crossing indicated BY4741 haploids to the BY4742 parental strain (ATCC, Manassas, VA) by mixing a bead of cells of each strain (from a single colony) together on a YPD plate and growing overnight at 30 °C. A small globule of this cell mixture was then re-streaked to single colonies on SD-Lys-Met agar plates to select for diploids.

Diploids constructed for the experiment presented in **Figure 4G** were made by crossing [*BIG*$^{+}$] or naïve haploids to the seamless GFP-Pus4 haploid strain. Due to incompatibility of auxotrophic makers, diploids could not be selected on dropout plates from cell mixtures. Instead, a pool of the mated cells was grown in several successive competitions to allow diploids to outcompete haploid parents. Diploids were then isolated from single colonies and imaged as described below.

Sporulations were performed inoculating single diploid colonies in Pre-SPO liquid media (YPD with 6% glucose) for 2 days at room temperature on a roller drum wheel. Cells were then pelleted and washed twice in SPO media (1% Potassium Acetate (Sigma, St. Louis, MO), 320 mg CSM-Met powder (Sunrise Scientific), 20 mg Methionine (Sigma) per liter), and then diluted ten-fold into 3 mL cultures of SPO. These cultures were incubated on a rotary wheel for one week at room temperature, before dissecting tetrads on a Singer Instruments MSM400 (Somerset, England).

The 3XFLAG-Pus4 strains were constructed using PCR combined with the "Delitto Perfetto" method (Storici and Resnick, 2006). Canavanine mutants were constructed by pelleting 500*u*L of a saturated YPD liquid culture, resuspending it in 100 *µ*LYPD and plating this on SD-Arg agar plates containing 60 *µg*/mL canavanine (Sigma), and growing for 2 days at 30°C. Single canavanine resistant colonies were picked and re-tested for resistance before further testing.

Cytoductions were performed as described in (Chakrabortee et al., 2016a). A BY4742 strain with a defective *KAR1* allele (*kar1-15*) was created as an initial recipient for cytoplasmic transfer. This allele prevents nuclear fusion during mating while permitting cytoplasmic transfer. The strain carries auxotrophic markers distinct from those in the putative [*BIG*$^{+}$] or naïve donor strains, and was also converted to petite with growth on ethidium bromide (strains were grown in YPD with 25ug/mL ethidium bromide for ~two-dozen generations before testing for growth on YP-glycerol). This allowed cytoplasmic transfer to be scored through the restoration of mitochondrial respiration, while selecting for auxotrophic markers unique to the recipient strain. The recipient and donor strains were mixed together on YPD-agar and grown overnight, followed by selection of heterokaryons and resulting haploid cytoductants on dropout media (selecting for the BY4742 recipient strain markers) containing glycerol as a carbon source. One more round of selection was used while replica-plating onto a dual-selection agar plate (SD-Lys-Met) to confirm that the colonies were not diploids. One additional round of propagation on a non-selective plate was performed before doing "reverse cytoductions," which were performed in the same way except selecting for

BY4741 auxotrophy in recipient naive strain. In the reverse cytoductions, the donors were naïve or putative-[*BIG*$^{+}$] BY4742 *kar1-15* cytoductants from the first round, and the recipients were wild-type or *pus4*Δ naïve BY4741 petite cells.

Transient *PUS4* deletion experiment strains were made by the Delitto Perfetto method (Storici and Resnick, 2006). After deletion of *PUS4*, strains were propagated for ~75 generations before phenotyping. The *PUS4* gene was re-introduced by homologous recombination.

Growth assays. Biological replicates of each yeast strain were pre-grown in rich media (YPD). We then diluted these saturated cultures 1:20 in sterile water and then inoculated 3 μL into 96-well humidified plates (Nunc Edge Plates (Thermo Scientific, Waltham, MA)) with 150 μL of YPD or SD-CSM per well. Cycloheximide (Sigma) was added to growth media at 0.05μg/mL. Rapamycin (LC Laboratories, Woburn, MA) was added to growth media at 10μM. Cell growth was monitored with continuous measurements of OD_{600} (~every 10 minutes) at 30°C over 96 hours using BioTek Eon or Synergy H1 microplate readers (Winooski, VT). Timepoints plotted in bar graphs correspond to the maximum proliferation rates calculated from growth data.

Measurement of chronological lifespan. For each strain, four single colonies were picked from freshly streaked YPD plate, and grown in 5mL of Pre-sporulation media for 3 days on a roller drum wheel (New Brunswick Scientific, Edison, NJ) at 30°C. Cultures were then pelleted and washed once with SPO media, and resuspended in 5mL of SPO

media, and placed back on the roller drum wheel at 30°C. On days indicated, a dilution was made of each replicate to achieve dozens to hundreds of colonies on a YPD plate, which were then counted using a colony counter (Synbiosos Acolyte, Frederick, MD). Dilution was ~100,000X at early stages of experiment, and later on was sometimes empirically determined after significant cell death. We note that aging the cells in SPO did not lead to significant acidification (pH of old cultures was found to be >5), as has been reported for cells aged in YPD, which contains high levels of glucose that upon metabolism leads to secretion of organic acids (Murakami et al., 2011).

Measurement of replicative lifespan. Replicative lifespan (RLS) was assessed using the standard method of isolating virgin cells on agar YPD (2% glucose) plates, and then separating their daughter cells at each cell division by micromanipulation and counting the total number of daughters produced by each mother cell (Steffen et al., 2009; Wasko et al., 2013). Strains were streaked from glycerol stocks onto YPD plates, and allowed to grow at 30°C until individual colonies could be selected for each strain. Colonies were lightly patched onto fresh YPD overnight and twenty cells were isolated by microdissection from each patch. These cells were incubated at 30°C for approximately two hours until they had formed daughter cells, at which time individual virgin daughter cells were selected and arrayed as previously described (Steffen et al., 2009) for lifespan analysis. From these, daughter cells were removed by microdissection and counted approximately every 2 hours during the day. Plates were maintained at 30°C during the day and placed at 4°C overnight. At least four

1169 independent replicates (arising from different colonies) of twenty individual mother cells
1170 each were measured for each strain.
1171
1172 **Curing**. Three regimes of chaperone inhibition were tested: 1) transient exposure to a
1173 dominant negative version of Hsp70 (Ssa1) to inhibit its activity (Chakrabortee et al.,
1174 2016a; Jarosz et al., 2014) 2) transient exposure to Radicicol (LC Laboratories) to
1175 inhibit Hsp90 activity (Chakrabortee et al., 2016a) 3) transient exposure to Guanidinium
1176 Hydrochloride (Sigma) to inhibit Hsp104 activity (Ferreira et al., 2001).
1177 Regime 1 was performed by transforming cells with a plasmid, PDJ169,
1178 harboring a dominant negative version of Hsp70 (Ssa1) as described previously
1179 (Chakrabortee et al., 2016a; Jarosz et al., 2014; Lagaudriere-Gesbert et al., 2002).
1180 Transformants were picked and re-streaked by hand or replica-pinned using a Singer
1181 HDA robot a total of twelve times on SD-Ura to promote $Ssa1^{DN}$ expression.
1182 (Anecdotally, we note that prion phenotypes are frequently cured with fewer than twelve
1183 restreasks, but for reasons of technical throughput, twelve were used in this
1184 experiment.) Then plasmids were eliminated by plating on media containing 5-fluoroortic
1185 acid (SD-Ura + 0.1% 5-FOA + 50 μg/mL uracil) and plasmid loss was verified by
1186 replating on SD-Ura. Colonies were then tested for elimination of prion phenotypes.
1187 Tested strains were compared to control strains that were restreaked in parallel on SD-
1188 CSM plates.
1189 Regime 2 was performed by replica-pinning cells six subsequent times on YPD
1190 agar plates containing 5 μM radicicol, using a Singer HDA robot. After re-platings, cells

were plated back onto YPD two subsequent times to facilitate recovery before being tested for elimination of prion phenotypes. Tested strains were compared to control strains that were replica-pinned in parallel on YPD plates.

Regime 3 was performed like Regime 2 but with SD-CSM plates containing 0.5 g/L Guanidinium Hydrochloride. Tested strains were compared to control strains that were replica-pinned in parallel on SD-CSM plates.

Wild yeast strains were cured by transforming a uracil-selectable 2micron plasmid (PDJ1222) encoding the aforementioned dominant negative version of Hsp70 (Ssa1), under control of a constituitive promoter (*pGPD*). Transformants were passaged on selective media five times to allow growth of single colonies. Transformants were then passaged three times on non-selective media (YPD) to permit plasmid loss, which was confirmed by the lack of growth on selective media (SD-Ura).

Strain competitions. Single colonies were used to inoculate 5 mL YPD cultures which were grown for 3 days on a roller drum wheel at 30°C. Cells were diluted 1000-fold and then mixed in equal volumes to form 50:50 mixtures of either of the following: Naïve Can^S and [*BIG*$^+$] Can^R; or Naïve Can^R and [*BIG*$^+$] Can^S. Before mixing cells, saturated cultures were measured to have near equal cell densities, and “time zero” measurement was made by plating the initial cell mixture and counting the number of Canavanine resistant colony forming units (CFUs) relative to total CFUs. These initial strain mixtures were then grown for 2 days on a roller drum wheel at 30°C, after which cells were diluted 50,000-fold or 25,000-fold and plated on YPD or canavanine plates, respectively.

These plates were grown at 30°C for 2 days before counting colonies. The liquid cultures were diluted 1:1000 in 5 mL of fresh YPD, and this process was repeated nine more times. Swapping of canavanine resistance between naïve and [*BIG*$^{+}$] was done to correct for the potential of canavanine resistance to influence cell growth, however in our experiments the differences were negligible. Numbers of canavanine-resistant and total colonies were compared relative to number of cells plated to determine the number of naïve or [*BIG*$^{+}$] colonies arising at each timepoint.

Microscopy and cell size measurements. Most microscopy was performed using a Leica inverted epifluorescence microscope (DMI6000B) with a Hammamatsu Orca 4.0 camera. Cells were imaged after 3 days of growth in 5 mL YPD at 30°C. Saturated cultures were diluted 10-fold with 1X PBS and briefly sonicated to break up cell clumps. Differential interference contrast (DIC) images were taken at 20 millisecond exposure time using a 63x/1.40 oil objective. Cell area was calculated using CellProfiler (3.1.5) image analysis software (www.cellprofiler.org)(Carpenter et al., 2006). Large cell threshold was set at one standard deviation above the cell area mean of the naïve cells.

GFP microscopy data presented in **Figure 4G** was imaged similarly to above, except that cells were grown in YPD for 24 hours.

Cell size experiments using protein synthesis inhibitors (**Fig. 6A–D**): Conditions were the same as above, with the following differences. Single colonies were inoculated into YPD, YPD+cycloheximide (0.05μg/mL), or YPD+rapamycin (10μM) and grown for 4 days before imaging. (Very similar results were observed after 3 days of growth.) The

following day, cultures were diluted into liquid YPD and grown for 3 days, after which they were restreaked once onto YPD agar. Single colonies were then used to inoculate liquid YPD cultures, grown for 3 days before imaging to test for the reappearance of the large cell size phenotype.

Data presented in **Figure 8C** was imaged similarly, except that cells were grown in SC-Ura media for retention of the GFP-Pus4 expression plasmid, and imaged using a GE DeltaVision Ultra microscope (Boston, MA).

Microscopy Image processing. ImageJ version 2.0.0-rc-69/1.52p, Build 269a0ad53f. For GFP-Pus4 in laboratory *S. cerevisiae* (**Fig. 4G**): 1) using full-size images, rolling background subtraction, radius of 50 pixels, 2) enhance contrast to allow 0.1% of pixels to be saturated, 3) check that brightness and contrast are adjusted equivalently in each image.

For GFP-Pus4 in wild *S. cerevisiae* isolate BC187 (**Fig. 8C**): 1) using full-size images, adjust brightness and contrast equivalently in both images, 2) set 50 x 50 pixel square in area between cells and measure average intensity, 3) subtract this intensity from the total image using the “Math” function.

Luciferase assays. Strains were transformed with PDJ512 and PDJ513. To maintain the plasmids, we grew these cells in a synthetic complete medium containing nutrient levels between those in SD and YPD formulations. Four independent transformants for each sample were grown for 1 day in 150 μL SC-Ura (Sunrise Scientific) per well in 96

well plates at 30°C. Saturated cultures were then diluted 15X into fresh media in a new 96 well plate and grown until cultures reach OD 0.6, as determined by a Biotek Eon plate reader. 20uL of each culture was added using multichannel pipette into a white flatbottom 96-well microplates (E&K Scientific, Santa Clara, CA) already containing 20uL of room temperature 1X Passive Lysis Buffer from the Dual Luciferase Reporter Assay System (Promega, Madison, WI). Cultures were then lysed by shaking at 300 rpm for 25 minutes at room temperature. *Renilla* and firefly luciferase activity was measured using and 75 μL injection volumes and otherwise default settings on a Veritas luminometer (Turner Biosystems). pTH726-CEN-RLuc/minCFLuc (PDJ512) and pTH727-CEN-RLuc/staCFLuc (PDJ513) were gifts from Tobias von der Haar (University of Kent)(Addgene plasmids # 38210 and # 38211) (Chu et al., 2014).

Final luciferase values were normalized to OD measurements of cultures to account for cell density. We note, however, that [*BIG*$^{+}$] cells did not have a general growth advantage over naïve cells in SC-Ura, and when comparing optical density measurements to those counting cells using a hemacytometer, we observed no perturbation in the relationship between cell number and optical density for [*BIG*$^{+}$] cells.

For wild strains, we considered the possibility that curing could reverse multiple epigenetic elements affecting plasmid copy number, transcription, or other elements of gene expression apart from protein synthesis. Indeed, after normalizing *Renilla* or firefly luciferase values to cell density, some strains have several fold-differences after curing, although they were closely correlated irrespective of which firefly codon variant was compared. Therefore, as for data presented in **Figure 6E,** for **Figure 8B** we also

normalized firefly luciferase values to *Renilla* luciferase, which is expressed from the same plasmid. This normalization procedure thus tests for differences in protein synthesis that are codon-frequency dependent, i.e. a measure of translational efficiency.

Polysome profiling. Single colonies from two biological replicates per sample were used to inoculate 5mL YPD cultures that were grown on a roller drum wheel at 30°C overnight. Saturated cultures were added to 95mL of YPD in 500 mL flasks and shaken at 225 rpm at 30°C until cultures reached OD 1.0. Five minutes prior to harvesting cells, we added cycloheximide (Sigma) to final concentration of 100 μg/mL to arrest translation, by adding 1 mL of a 10 mg/mL stock solution (in ethanol) per culture, then immediately swirling flask and putting back on shaker for 5 minutes 225 rpm 30°C to permit the chemical to enter cells and arrest protein synthesis. Cultures were pelleted in 50 mL conical tubes for 3 minutes at 5000 rpm. After decanting supernatant, pellets were quickly resuspend in ice-cold Polysome Lysis Buffer (Jan et al., 2014) (PLB)(20 mM Tris pH 8.0, 140 mM KCl, 1.5 mM MgCl2, 100 μg/mL cycloheximide, 1% Triton X-100, RNase-free reagents), 250 μL total PLB per sample. Resuspended pellets were then flash frozen in liquid nitrogen. Pellets were weighed to ensure their weights were near equal, and then thawed on ice. 250μL of additional ice cold PLB was added per sample, making slightly over 0.5 mL per sample. Samples were then flash frozen in tiny pellets ("yeast dippin' dots") by pipetting directly into a small dewar filled with liquid nitrogen and a wire mesh basket nested inside. Tiny pellets were then stored at -80°C until lysis. Samples were lysed using a Retsch Cryomill (Haan, Germany) with 25 mL canisters

and the following program: pre-cool, then 12 cycles of 15 Hz x 3 minutes. Smears of lysate were stained with Trypan blue and imaged under a microscope to verify efficient lysis. (We suspect with larger sample volume:canister volume ratios, fewer cycles would be necessary.)

Lysates were loaded onto 10–50% sucrose gradients pre-poured on a BioComp Gradient Master 108 (Fredericton, ND, Canada). Lysates generally contained RNA concentrations around 12–18 μg/μL. 30 μL of lysate was carefully pipetted onto the top of the sucrose gradient, and samples were spun in a Beckman SW41 Ti Rotor for 2.5 hours at 4°C at 40,000 rpm. Gradients were analyzed on Brandel fractionator (Gaithersburg, MD). Technical replicates (same lysate independently loaded onto separate gradients) showed a very high degree of similarity, as did biological replicates.

GFP-fusion measurements. Naïve or [*BIG*$^{+}$] cells were mated to the SWAT seamless-GFP library (Weill et al., 2018; Yofe et al., 2016) on solid YPD agar plates in 384-spot format for 24 hours at room temperature. Diploids were selected on media lacking both lysine and methionine (SD-Lys-Met) and propagated for 48 hour at room temperature. Diploids were inncoulated into 60 μL of liquid media lacking both lysine and methionine (SD-Lys-Met) in 384-well plates. All library manipulations were carried out using a Singer ROTOR HDA robotic pinning instrument. Cells were propagated in liquid medium for 24 hours at 30°C (OD_{600} ~ 1), at which time OD_{600} and green fluorescence were measured using a BioTek Synergy H1 plate reader. OD_{600} was adjusted based on

known blank wells, and the GFP/OD600 measurements were normalized by Z-score ([x_i - μ]/σ) within the naïve and [*BIG*$^+$] populations independently.

Western blots. For SDS-PAGE, immunoblots and protein yield measurements, cells were lysed using a Retsch Cryomill using the following program: six 3-minute cycles at 15Hz with 2-minute cooling cycles in between. Cell lysates were loaded onto GenScript ExpressPlus SDS-PAGE 4–20% gels (Piscataway, NJ) and stained using coomassie blue. For Western Blots, anti-FLAG M2 monoclonal antibody (Sigma) was used to detect 3XFLAG-Pus4, and anti-PGK1 monoclonal antibody (Invitrogen) was used to detect the loading control.

RNA-sequencing. Five independent colonies of naïve and [*BIG*$^+$] cells were grown in 5 mL YPD cultures on a culture roller drum wheel overnight at 30°C. Saturated cultures were added to 700 mL YPD cultures in 2 L narrow mouthed baffled flasks, pre-incubated to 30°C. These were grown until a cuvette reading of OD 1.0. (700 mL cultures were used to provide enough material for other sample-intensive experiments done in parallel). Cultures were pelleted in large table-top centrifuge with swing-bucket rotor at 4300 x g at 4°C for 20 minutes, washing once with ice-cold 1X TBS. RNA was harvested as described in (Carlile et al., 2015). Total RNA was treated with RiboZero (Illumina, San Diego, CA) to remove most rRNAs but retain mRNAs and other ncRNAs. RNA was fragmented and submitted for Illumina sequencing at the Beijing Genomics Institute. Analysis was performed using Bowtie2 (Langmead and Salzberg, 2012), HT-

Seq (Anders et al., 2015), and DE-Seq2 (Love et al., 2014). Raw data and other experimental information are available on the Gene Expression Omnibus (Barrett et al., 2013), accession:

https://www.ncbi.nlm.nih.gov/geo/query/acc.cgi?acc=GSE153930

tRNA/rRNA quantification. Strains were grown up in 5mL of YPD overnight at 30°C. Saturated cultures were then diluted 15X into fresh media and grown up to an OD 0.8. Cells were then pelleted, and total RNA was extracted by phenol-chloroform extraction. RNA concentration for each sample was then analyzed on Nanodrop, and diluted to equal concentrations in RNase-free water. The extracted RNA was then run on nucleic acid fragment analyzer, and total tRNA abundance was quantified relative to abundance of 5.8S rRNA.

Pseudouridine measurements. Protocol adapted from reference (Lei and Yi, 2017). For each sample, 40 μg of total RNA was fragmented in RNA fragmentation buffer (New England Bio Labs, Ipswich, MA) at 94°C for 3 min. Following ethanol precipitation, fragmented RNA was resuspended in 80 μL of 5 mM EDTA, denatured at 80°C for 5 min, and then immediately chilled on ice. Each sample was then split into two 40 μL samples for a CMC-labeled and non-labeled control. The 40 μL RNA sample destined for CMC-labeling was added to 400 μL BEU+CMC buffer (50 mM Bicine, pH 8.5; 4 mM EDTA; 7 M urea; 200 mM CMC (Sigma)). The non-labeled 40 μL RNA sample was added to 400μL BEu buffer (50 mM Bicine, pH 8.5; 4 mM EDTA; 7 M urea). Both samples were incubated at 37°C for 20 min to carry out the CMC-Ψ reaction, followed

by an ethanol precipitation. Each sample was then resuspended in 200 μL Na_2CO_3 buffer (50 mM Na_2CO_3, pH 10.4; 2 mM EDTA) and incubated at 37°C for 6 h. Following incubation, RNA was ethanol precipitated and resuspended in 40 μL H2O. RNA was annealed to primers by the addition of 4 μL 100 μM Random Hexamer Primers (TaKaRa, Mountain View, CA) and incubation at 65°C for 5 min. Samples were chilled on ice afterwards. To perform the reverse transcription, 32 μL RT Buffer (125 mM Tris, pH 8.0; 15 mM $MnCl_2$; 187.5 mM KCl; 1.25 mM dNTPs; 25mM DTT) was added to each sample. Samples were then incubated at 25°C for 2 min. After, 0.5 μL SuperScript II reverse transcriptase (SSII, Invitrogen, Waltham, MA) was added to each sample followed by incubation at 25°C for 10 min, 42°C for 3 h, and 70°C for 15 min. To perform qPCR analysis, 2 μL of sample was mixed with 10 μL 2X SYBR Mix (Kapa Biosystems, Wilmington, MA), 0.4 μL of each 10 μM primer (IDT, Coralville, IA), and 7.2 μL H2O for a total of 20 μL for each reaction. qPCR was performed in a Bio-Rad CFX Connect Real-Time System (Bio-Rad, Hercules, CA) using the following protocol: initial incubation at 95°C for 5 min, followed by 45 cycles of 95°C for 0.5 min and 60°C for 1 min. Following amplification, reaction was brought down to 54°C and held for 5s, increasing in temperature by 0.1°C increments until 95°C is reached to obtain melt curve data.

Data display. Plots/graphs were made using PRISM 7/8 software (GraphPad, San Diego, CA).

REFERENCES

Alberti, S., Halfmann, R., King, O., Kapila, A., and Lindquist, S. (2009). A systematic survey identifies prions and illuminates sequence features of prionogenic proteins. Cell *137*, 146-158.

Ali, M., Chernova, T.A., Newnam, G.P., Yin, L., Shanks, J., Karpova, T.S., Lee, A., Laur, O., Subramanian, S., Kim, D.*, et al.* (2014). Stress-dependent proteolytic processing of the actin assembly protein Lsb1 modulates a yeast prion. J Biol Chem *289*, 27625-27639.

Anders, S., Pyl, P.T., and Huber, W. (2015). HTSeq--a Python framework to work with high-throughput sequencing data. Bioinformatics *31*, 166-169.

Anzi, S., Stolovich-Rain, M., Klochendler, A., Fridlich, O., Helman, A., Paz-Sonnenfeld, A., Avni-Magen, N., Kaufman, E., Ginzberg, M.B., Snider, D.*, et al.* (2018). Postnatal Exocrine Pancreas Growth by Cellular Hypertrophy Correlates with a Shorter Lifespan in Mammals. Dev Cell *45*, 726-737 e723.

Bailey, T.L., Boden, M., Buske, F.A., Frith, M., Grant, C.E., Clementi, L., Ren, J., Li, W.W., and Noble, W.S. (2009). MEME SUITE: tools for motif discovery and searching. Nucleic acids research *37*, W202-208.

Baliga, B.S., Pronczuk, A.W., and Munro, H.N. (1969). Mechanism of cycloheximide inhibition of protein synthesis in a cell-free system prepared from rat liver. J Biol Chem *244*, 4480-4489.

Barrett, T., Wilhite, S.E., Ledoux, P., Evangelista, C., Kim, I.F., Tomashevsky, M., Marshall, K.A., Phillippy, K.H., Sherman, P.M., Holko, M.*, et al.* (2013). NCBI GEO: archive for functional genomics data sets--update. Nucleic acids research *41*, D991-995.

Baudin-Baillieu, A., Legendre, R., Kuchly, C., Hatin, I., Demais, S., Mestdagh, C., Gautheret, D., and Namy, O. (2014). Genome-wide translational changes induced by the prion [PSI+]. Cell Rep *8*, 439-448.

Becker, H.F., Motorin, Y., Planta, R.J., and Grosjean, H. (1997). The yeast gene YNL292w encodes a pseudouridine synthase (Pus4) catalyzing the formation of psi55 in both mitochondrial and cytoplasmic tRNAs. Nucleic acids research *25*, 4493-4499.

Beretta, L., Gingras, A.C., Svitkin, Y.V., Hall, M.N., and Sonenberg, N. (1996). Rapamycin blocks the phosphorylation of 4E-BP1 and inhibits cap-dependent initiation of translation. EMBO J *15*, 658-664.

Bitto, A., Wang, A.M., Bennett, C.F., and Kaeberlein, M. (2015). Biochemical Genetic Pathways that Modulate Aging in Multiple Species. Cold Spring Harb Perspect Med *5*.

1423 Bjedov, I., Toivonen, J.M., Kerr, F., Slack, C., Jacobson, J., Foley, A., and Partridge, L.
1424 (2010). Mechanisms of life span extension by rapamycin in the fruit fly Drosophila
1425 melanogaster. Cell Metab *11*, 35-46.

1426 Breslow, D.K., Cameron, D.M., Collins, S.R., Schuldiner, M., Stewart-Ornstein, J.,
1427 Newman, H.W., Braun, S., Madhani, H.D., Krogan, N.J., and Weissman, J.S. (2008). A
1428 comprehensive strategy enabling high-resolution functional analysis of the yeast
1429 genome. Nat Methods *5*, 711-718.

1430 Broach, J.R. (2012). Nutritional control of growth and development in yeast. Genetics
1431 *192*, 73-105.

1432 Brown, J.C., and Lindquist, S. (2009). A heritable switch in carbon source utilization
1433 driven by an unusual yeast prion. Genes Dev *23*, 2320-2332.

1434 Butcher, R.A., Bhullar, B.S., Perlstein, E.O., Marsischky, G., LaBaer, J., and Schreiber,
1435 S.L. (2006). Microarray-based method for monitoring yeast overexpression strains
1436 reveals small-molecule targets in TOR pathway. Nat Chem Biol *2*, 103-109.

1437 Byers, J.S., and Jarosz, D.F. (2014). Pernicious pathogens or expedient elements of
1438 inheritance: the significance of yeast prions. PLoS Pathog *10*, e1003992.

1439 Carlile, T.M., Rojas-Duran, M.F., and Gilbert, W.V. (2015). Pseudo-Seq: Genome-Wide
1440 Detection of Pseudouridine Modifications in RNA. Methods Enzymol *560*, 219-245.

1441 Carlile, T.M., Rojas-Duran, M.F., Zinshteyn, B., Shin, H., Bartoli, K.M., and Gilbert, W.V.
1442 (2014). Pseudouridine profiling reveals regulated mRNA pseudouridylation in yeast and
1443 human cells. Nature *515*, 143-146.

1444 Carpenter, A.E., Jones, T.R., Lamprecht, M.R., Clarke, C., Kang, I.H., Friman, O.,
1445 Guertin, D.A., Chang, J.H., Lindquist, R.A., Moffat, J.*, et al.* (2006). CellProfiler: image
1446 analysis software for identifying and quantifying cell phenotypes. Genome Biol *7*, R100.

1447 Catania, S., Dumesic, P.A., Pimentel, H., Nasif, A., Stoddard, C.I., Burke, J.E., Diedrich,
1448 J.K., Cook, S., Shea, T., Geinger, E.*, et al.* (2020). Evolutionary Persistence of DNA
1449 Methylation for Millions of Years after Ancient Loss of a De Novo Methyltransferase.
1450 Cell *180*, 263-277 e220.

1451 Chakrabortee, S., Byers, J.S., Jones, S., Garcia, D.M., Bhullar, B., Chang, A., She, R.,
1452 Lee, L., Fremin, B., Lindquist, S.*, et al.* (2016a). Intrinsically Disordered Proteins Drive
1453 Emergence and Inheritance of Biological Traits. Cell *167*, 369-381 e312.

1454 Chakrabortee, S., Kayatekin, C., Newby, G.A., Mendillo, M.L., Lancaster, A., and
1455 Lindquist, S. (2016b). Luminidependens (LD) is an Arabidopsis protein with prion
1456 behavior. Proc Natl Acad Sci U S A *113*, 6065-6070.

1457 Chakravarty, A.K., Smejkal, T., Itakura, A.K., Garcia, D.M., and Jarosz, D.F. (2019). A
1458 Non-amyloid Prion Particle that Activates a Heritable Gene Expression Program. Mol
1459 Cell.

1460 Chernoff, Y.O., Lindquist, S.L., Ono, B., Inge-Vechtomov, S.G., and Liebman, S.W.
1461 (1995). Role of the chaperone protein Hsp104 in propagation of the yeast prion-like
1462 factor [psi+]. Science *268*, 880-884.

1463 Cherry, J.M., Hong, E.L., Amundsen, C., Balakrishnan, R., Binkley, G., Chan, E.T.,
1464 Christie, K.R., Costanzo, M.C., Dwight, S.S., Engel, S.R.*, et al.* (2012). Saccharomyces
1465 Genome Database: the genomics resource of budding yeast. Nucleic acids research *40*,
1466 D700-705.

1467 Chu, D., Kazana, E., Bellanger, N., Singh, T., Tuite, M.F., and von der Haar, T. (2014).
1468 Translation elongation can control translation initiation on eukaryotic mRNAs. EMBO J
1469 *33*, 21-34.

1470 Chung, J., Kuo, C.J., Crabtree, G.R., and Blenis, J. (1992). Rapamycin-FKBP
1471 specifically blocks growth-dependent activation of and signaling by the 70 kd S6 protein
1472 kinases. Cell *69*, 1227-1236.

1473 Cox, B.S. (1965). A cytoplasmic supressor of a super-supressor in yeast. Heredity *20*,
1474 505–521.

1475 Cubillos, F.A., Louis, E.J., and Liti, G. (2009). Generation of a large set of genetically
1476 tractable haploid and diploid Saccharomyces strains. FEMS Yeast Res *9*, 1217-1225.

1477 Dikicioglu, D., Dereli Eke, E., Eraslan, S., Oliver, S.G., and Kirdar, B. (2018).
1478 Saccharomyces cerevisiae adapted to grow in the presence of low-dose rapamycin
1479 exhibit altered amino acid metabolism. Cell Commun Signal *16*, 85.

1480 Dreher, T.W., Uhlenbeck, O.C., and Browning, K.S. (1999). Quantitative assessment of
1481 EF-1alpha.GTP binding to aminoacyl-tRNAs, aminoacyl-viral RNA, and tRNA shows
1482 close correspondence to the RNA binding properties of EF-Tu. J Biol Chem *274*, 666-
1483 672.

1484 Dudley, A.M., Janse, D.M., Tanay, A., Shamir, R., and Church, G.M. (2005). A global
1485 view of pleiotropy and phenotypically derived gene function in yeast. Mol Syst Biol *1*,
1486 2005 0001.

1487 Eaglestone, S.S., Ruddock, L.W., Cox, B.S., and Tuite, M.F. (2000). Guanidine
1488 hydrochloride blocks a critical step in the propagation of the prion-like determinant
1489 [PSI(+)] of Saccharomyces cerevisiae. Proc Natl Acad Sci U S A *97*, 240-244.

1490 Ecker, R.E., and Schaechter, M. (1963). Ribosome Content and the Rate of Growth of
1491 Salmonella Typhimurium. Biochim Biophys Acta *76*, 275-279.

1492 Efeyan, A., Comb, W.C., and Sabatini, D.M. (2015). Nutrient-sensing mechanisms and
1493 pathways. Nature *517*, 302-310.

1494 Egilmez, N.K., Chen, J.B., and Jazwinski, S.M. (1990). Preparation and partial
1495 characterization of old yeast cells. J Gerontol *45*, B9-17.

1496 Eyler, D.E., Franco, M.K., Batool, Z., Wu, M.Z., Dubuke, M.L., Dobosz-Bartoszek, M.,
1497 Jones, J.D., Polikanov, Y.S., Roy, B., and Koutmou, K.S. (2019). Pseudouridinylation of
1498 mRNA coding sequences alters translation. Proc Natl Acad Sci U S A *116*, 23068-
1499 23074.

1500 Fabrizio, P., Pozza, F., Pletcher, S.D., Gendron, C.M., and Longo, V.D. (2001).
1501 Regulation of longevity and stress resistance by Sch9 in yeast. Science *292*, 288-290.

1502 Ferreira, P.C., Ness, F., Edwards, S.R., Cox, B.S., and Tuite, M.F. (2001). The
1503 elimination of the yeast [PSI+] prion by guanidine hydrochloride is the result of Hsp104
1504 inactivation. Mol Microbiol *40*, 1357-1369.

1505 Fingar, D.C., Salama, S., Tsou, C., Harlow, E., and Blenis, J. (2002). Mammalian cell
1506 size is controlled by mTOR and its downstream targets S6K1 and 4EBP1/eIF4E. Genes
1507 Dev *16*, 1472-1487.

1508 Fontana, L., Partridge, L., and Longo, V.D. (2010). Extending healthy life span--from
1509 yeast to humans. Science *328*, 321-326.

1510 Frumkin, I., Lajoie, M.J., Gregg, C.J., Hornung, G., Church, G.M., and Pilpel, Y. (2018).
1511 Codon usage of highly expressed genes affects proteome-wide translation efficiency.
1512 Proc Natl Acad Sci U S A *115*, E4940-E4949.

1513 Garay, E., Campos, S.E., Gonzalez de la Cruz, J., Gaspar, A.P., Jinich, A., and Deluna,
1514 A. (2014). High-resolution profiling of stationary-phase survival reveals yeast longevity
1515 factors and their genetic interactions. PLoS Genet *10*, e1004168.

1516 Garcia, D.M., Dietrich, D., Clardy, J., and Jarosz, D.F. (2016). A common bacterial
1517 metabolite elicits prion-based bypass of glucose repression. Elife *5*.

1518 Garcia, D.M., and Jarosz, D.F. (2014). Rebels with a cause: molecular features and
1519 physiological consequences of yeast prions. FEMS Yeast Res *14*, 136-147.

1520 Gietz, D., St Jean, A., Woods, R.A., and Schiestl, R.H. (1992). Improved method for
1521 high efficiency transformation of intact yeast cells. Nucleic Acids Res *20*, 1425.

1522 Gingold, H., and Pilpel, Y. (2011). Determinants of translation efficiency and accuracy.
1523 Mol Syst Biol *7*, 481.

1524 Grewal, S.I., and Klar, A.J. (1996). Chromosomal inheritance of epigenetic states in
1525 fission yeast during mitosis and meiosis. Cell *86*, 95-101.

Gutgsell, N., Englund, N., Niu, L., Kaya, Y., Lane, B.G., and Ofengand, J. (2000). Deletion of the Escherichia coli pseudouridine synthase gene truB blocks formation of pseudouridine 55 in tRNA in vivo, does not affect exponential growth, but confers a strong selective disadvantage in competition with wild-type cells. RNA *6*, 1870-1881.

Halfmann, R., Jarosz, D.F., Jones, S.K., Chang, A., Lancaster, A.K., and Lindquist, S. (2012). Prions are a common mechanism for phenotypic inheritance in wild yeasts. Nature *482*, 363-368.

Hanahan, D., and Weinberg, R.A. (2011). Hallmarks of cancer: the next generation. Cell *144*, 646-674.

Harrison, D.E., Strong, R., Sharp, Z.D., Nelson, J.F., Astle, C.M., Flurkey, K., Nadon, N.L., Wilkinson, J.E., Frenkel, K., Carter, C.S.*, et al.* (2009). Rapamycin fed late in life extends lifespan in genetically heterogeneous mice. Nature *460*, 392-395.

Harvey, S.L., and Kellogg, D.R. (2003). Conservation of mechanisms controlling entry into mitosis: budding yeast wee1 delays entry into mitosis and is required for cell size control. Curr Biol *13*, 264-275.

Harvey, Z.H., Chen, Y., and Jarosz, D.F. (2018). Protein-Based Inheritance: Epigenetics beyond the Chromosome. Mol Cell *69*, 195-202.

He, C., Tsuchiyama, S.K., Nguyen, Q.T., Plyusnina, E.N., Terrill, S.R., Sahibzada, S., Patel, B., Faulkner, A.R., Shaposhnikov, M.V., Tian, R.*, et al.* (2014). Enhanced longevity by ibuprofen, conserved in multiple species, occurs in yeast through inhibition of tryptophan import. PLoS Genet *10*, e1004860.

Heard, E., and Martienssen, R.A. (2014). Transgenerational epigenetic inheritance: myths and mechanisms. Cell *157*, 95-109.

Hughes, K.A., and Reynolds, R.M. (2005). Evolutionary and mechanistic theories of aging. Annu Rev Entomol *50*, 421-445.

Huh, W.K., Falvo, J.V., Gerke, L.C., Carroll, A.S., Howson, R.W., Weissman, J.S., and O'Shea, E.K. (2003). Global analysis of protein localization in budding yeast. Nature *425*, 686-691.

Itakura, A.K., Chakravarty, A.K., Jakobson, C.M., and Jarosz, D.F. (2019). Widespread Prion-Based Control of Growth and Differentiation Strategies in Saccharomyces cerevisiae. Mol Cell.

Ivanov, D.K., Escott-Price, V., Ziehm, M., Magwire, M.M., Mackay, T.F., Partridge, L., and Thornton, J.M. (2015). Longevity GWAS Using the Drosophila Genetic Reference Panel. J Gerontol A Biol Sci Med Sci *70*, 1470-1478.

Jakobson, C.M., and Jarosz, D.F. (2019). Molecular Origins of Complex Heritability in Natural Genotype-to-Phenotype Relationships. Cell Syst *8*, 363-379 e363.

Jakobson, C.M., She, R., and Jarosz, D.F. (2019). Pervasive function and evidence for selection across standing genetic variation in S. cerevisiae. Nat Commun *10*, 1222.

Jan, C.H., Williams, C.C., and Weissman, J.S. (2014). Principles of ER cotranslational translocation revealed by proximity-specific ribosome profiling. Science *346*, 1257521.

Janssens, G.E., Meinema, A.C., Gonzalez, J., Wolters, J.C., Schmidt, A., Guryev, V., Bischoff, R., Wit, E.C., Veenhoff, L.M., and Heinemann, M. (2015). Protein biogenesis machinery is a driver of replicative aging in yeast. Elife *4*, e08527.

Jarosz, D.F., Lancaster, A.K., Brown, J.C.S., and Lindquist, S. (2014). An evolutionarily conserved prion-like element converts wild fungi from metabolic specialists to generalists. Cell *158*, 1072-1082.

Johnston, G.C., Pringle, J.R., and Hartwell, L.H. (1977). Coordination of growth with cell division in the yeast Saccharomyces cerevisiae. Exp Cell Res *105*, 79-98.

Jorgensen, P., Nishikawa, J.L., Breitkreutz, B.J., and Tyers, M. (2002). Systematic identification of pathways that couple cell growth and division in yeast. Science *297*, 395-400.

Jorgensen, P., and Tyers, M. (2004). How cells coordinate growth and division. Curr Biol *14*, R1014-1027.

Jung, P.P., Zhang, Z., Paczia, N., Jaeger, C., Ignac, T., May, P., and Linster, C.L. (2018). Natural variation of chronological aging in the Saccharomyces cerevisiae species reveals diet-dependent mechanisms of life span control. NPJ Aging Mech Dis *4*, 3.

Kabani, M., Redeker, V., and Melki, R. (2014). A role for the proteasome in the turnover of Sup35p and in [PSI(+)] prion propagation. Mol Microbiol *92*, 507-528.

Kaeberlein, M. (2010). Lessons on longevity from budding yeast. Nature *464*, 513-519.

Kaeberlein, M., and Kennedy, B.K. (2007). Protein translation, 2007. Aging Cell *6*, 731-734.

Kaeberlein, M., Kirkland, K.T., Fields, S., and Kennedy, B.K. (2005). Genes determining yeast replicative life span in a long-lived genetic background. Mech Ageing Dev *126*, 491-504.

Kaeberlein, M., McVey, M., and Guarente, L. (1999). The SIR2/3/4 complex and SIR2 alone promote longevity in Saccharomyces cerevisiae by two different mechanisms. Genes Dev *13*, 2570-2580.

1594 Kafri, M., Metzl-Raz, E., Jona, G., and Barkai, N. (2016). The Cost of Protein
1595 Production. Cell Rep *14*, 22-31.

1596 Kapitzky, L., Beltrao, P., Berens, T.J., Gassner, N., Zhou, C., Wuster, A., Wu, J., Babu,
1597 M.M., Elledge, S.J., Toczyski, D.*, et al.* (2010). Cross-species chemogenomic profiling
1598 reveals evolutionarily conserved drug mode of action. Mol Syst Biol *6*, 451.

1599 Kariko, K., Muramatsu, H., Welsh, F.A., Ludwig, J., Kato, H., Akira, S., and Weissman,
1600 D. (2008). Incorporation of pseudouridine into mRNA yields superior nonimmunogenic
1601 vector with increased translational capacity and biological stability. Mol Ther *16*, 1833-
1602 1840.

1603 Kaya, A., Ma, S., Wasko, B., Lee, M., Kaeberlein, M., and Gladyshev, V.N. (2015).
1604 Defining Molecular Basis for Longevity Traits in Natural Yeast Isolates. NPJ Aging Mech
1605 Dis *1*.

1606 Keffer-Wilkes, L.C., Veerareddygari, G.R., and Kothe, U. (2016). RNA modification
1607 enzyme TruB is a tRNA chaperone. Proc Natl Acad Sci U S A *113*, 14306-14311.

1608 Kenyon, C.J. (2010). The genetics of ageing. Nature *464*, 504-512.

1609 Kertesz, M., Wan, Y., Mazor, E., Rinn, J.L., Nutter, R.C., Chang, H.Y., and Segal, E.
1610 (2010). Genome-wide measurement of RNA secondary structure in yeast. Nature *467*,
1611 103-107.

1612 King, O.D., and Masel, J. (2007). The evolution of bet-hedging adaptations to rare
1613 scenarios. Theor Popul Biol *72*, 560-575.

1614 Krogan, N.J., Cagney, G., Yu, H., Zhong, G., Guo, X., Ignatchenko, A., Li, J., Pu, S.,
1615 Datta, N., Tikuisis, A.P.*, et al.* (2006). Global landscape of protein complexes in the
1616 yeast Saccharomyces cerevisiae. Nature *440*, 637-643.

1617 Kuo, C.J., Chung, J., Fiorentino, D.F., Flanagan, W.M., Blenis, J., and Crabtree, G.R.
1618 (1992). Rapamycin selectively inhibits interleukin-2 activation of p70 S6 kinase. Nature
1619 *358*, 70-73.

1620 Kwan, E.X., Foss, E., Kruglyak, L., and Bedalov, A. (2011). Natural polymorphism in
1621 BUL2 links cellular amino acid availability with chronological aging and telomere
1622 maintenance in yeast. PLoS Genet *7*, e1002250.

1623 Kyte, J., and Doolittle, R.F. (1982). A simple method for displaying the hydropathic
1624 character of a protein. J Mol Biol *157*, 105-132.

1625 Lagaudriere-Gesbert, C., Newmyer, S.L., Gregers, T.F., Bakke, O., and Ploegh, H.L.
1626 (2002). Uncoating ATPase Hsc70 is recruited by invariant chain and controls the size of
1627 endocytic compartments. Proc Natl Acad Sci U S A *99*, 1515-1520.

1628 Landry, C.R., Townsend, J.P., Hartl, D.L., and Cavalieri, D. (2006). Ecological and
1629 evolutionary genomics of Saccharomyces cerevisiae. Mol Ecol *15*, 575-591.

1630 Langmead, B., and Salzberg, S.L. (2012). Fast gapped-read alignment with Bowtie 2.
1631 Nat Methods *9*, 357-359.

1632 Lei, Z., and Yi, C. (2017). A Radiolabeling-Free, qPCR-Based Method for Locus-
1633 Specific Pseudouridine Detection. Angew Chem Int Ed Engl *56*, 14878-14882.

1634 Li, C., Qian, W., Maclean, C.J., and Zhang, J. (2016). The fitness landscape of a tRNA
1635 gene. Science *352*, 837-840.

1636 Li, L., and Kowal, A.S. (2012). Environmental regulation of prions in yeast. PLoS Pathog
1637 *8*, e1002973.

1638 Liebman, S.W., and Chernoff, Y.O. (2012). Prions in yeast. Genetics *191*, 1041-1072.

1639 Lloyd, A.C. (2013). The regulation of cell size. Cell *154*, 1194-1205.

1640 Longo, V.D., Shadel, G.S., Kaeberlein, M., and Kennedy, B. (2012). Replicative and
1641 chronological aging in Saccharomyces cerevisiae. Cell Metab *16*, 18-31.

1642 Love, M.I., Huber, W., and Anders, S. (2014). Moderated estimation of fold change and
1643 dispersion for RNA-seq data with DESeq2. Genome Biol *15*, 550.

1644 Lovejoy, A.F., Riordan, D.P., and Brown, P.O. (2014). Transcriptome-wide mapping of
1645 pseudouridines: pseudouridine synthases modify specific mRNAs in S. cerevisiae.
1646 PLoS One *9*, e110799.

1647 Marek, A., and Korona, R. (2013). Restricted pleiotropy facilitates mutational erosion of
1648 major life-history traits. Evolution *67*, 3077-3086.

1649 Martinez-Outschoorn, U.E., Peiris-Pages, M., Pestell, R.G., Sotgia, F., and Lisanti, M.P.
1650 (2017). Cancer metabolism: a therapeutic perspective. Nat Rev Clin Oncol *14*, 11-31.

1651 McCormick, M.A., Delaney, J.R., Tsuchiya, M., Tsuchiyama, S., Shemorry, A., Sim, S.,
1652 Chou, A.C., Ahmed, U., Carr, D., Murakami, C.J.*, et al.* (2015). A Comprehensive
1653 Analysis of Replicative Lifespan in 4,698 Single-Gene Deletion Strains Uncovers
1654 Conserved Mechanisms of Aging. Cell Metab *22*, 895-906.

1655 McKeehan, W., and Hardesty, B. (1969). The mechanism of cycloheximide inhibition of
1656 protein synthesis in rabbit reticulocytes. Biochem Biophys Res Commun *36*, 625-630.

1657 McKinley, M.P., Bolton, D.C., and Prusiner, S.B. (1983). A protease-resistant protein is
1658 a structural component of the scrapie prion. Cell *35*, 57-62.

1659 Moazed, D. (2011). Mechanisms for the inheritance of chromatin states. Cell *146*, 510-
1660 518.

1661 Murakami, C.J., Wall, V., Basisty, N., and Kaeberlein, M. (2011). Composition and
1662 acidification of the culture medium influences chronological aging similarly in vineyard
1663 and laboratory yeast. PLoS One *6*, e24530.

1664 Nakamoto, M.A., Lovejoy, A.F., Cygan, A.M., and Boothroyd, J.C. (2017). mRNA
1665 pseudouridylation affects RNA metabolism in the parasite Toxoplasma gondii. RNA *23*,
1666 1834-1849.

1667 Nakayama, J., Klar, A.J., and Grewal, S.I. (2000). A chromodomain protein, Swi6,
1668 performs imprinting functions in fission yeast during mitosis and meiosis. Cell *101*, 307-
1669 317.

1670 Neurohr, G.E., Terry, R.L., Lengefeld, J., Bonney, M., Brittingham, G.P., Moretto, F.,
1671 Miettinen, T.P., Vaites, L.P., Soares, L.M., Paulo, J.A.*, et al.* (2019). Excessive Cell
1672 Growth Causes Cytoplasm Dilution And Contributes to Senescence. Cell *176*, 1083-
1673 1097 e1018.

1674 Noll, H. (2008). The discovery of polyribosomes. Bioessays *30*, 1220-1234.

1675 Perlstein, D.L., Ge, J., Ortigosa, A.D., Robblee, J.H., Zhang, Z., Huang, M., and Stubbe,
1676 J. (2005). The active form of the Saccharomyces cerevisiae ribonucleotide reductase
1677 small subunit is a heterodimer in vitro and in vivo. Biochemistry *44*, 15366-15377.

1678 Pitt, J.N., and Kaeberlein, M. (2015). Why is aging conserved and what can we do
1679 about it? PLoS Biol *13*, e1002131.

1680 Plotkin, J.B., and Kudla, G. (2011). Synonymous but not the same: the causes and
1681 consequences of codon bias. Nat Rev Genet *12*, 32-42.

1682 Polymenis, M., and Schmidt, E.V. (1997). Coupling of cell division to cell growth by
1683 translational control of the G1 cyclin CLN3 in yeast. Genes Dev *11*, 2522-2531.

1684 Powers, R.W., 3rd, Kaeberlein, M., Caldwell, S.D., Kennedy, B.K., and Fields, S.
1685 (2006). Extension of chronological life span in yeast by decreased TOR pathway
1686 signaling. Genes Dev *20*, 174-184.

1687 Price, D.J., Grove, J.R., Calvo, V., Avruch, J., and Bierer, B.E. (1992). Rapamycin-
1688 induced inhibition of the 70-kilodalton S6 protein kinase. Science *257*, 973-977.

1689 Robichaud, N., Sonenberg, N., Ruggero, D., and Schneider, R.J. (2019). Translational
1690 Control in Cancer. Cold Spring Harb Perspect Biol *11*.

1691 Robida-Stubbs, S., Glover-Cutter, K., Lamming, D.W., Mizunuma, M., Narasimhan,
1692 S.D., Neumann-Haefelin, E., Sabatini, D.M., and Blackwell, T.K. (2012). TOR signaling

and rapamycin influence longevity by regulating SKN-1/Nrf and DAF-16/FoxO. Cell Metab *15*, 713-724.

Safra, M., Nir, R., Farouq, D., Vainberg Slutskin, I., and Schwartz, S. (2017). TRUB1 is the predominant pseudouridine synthase acting on mammalian mRNA via a predictable and conserved code. Genome Res *27*, 393-406.

Sarin, L.P., and Leidel, S.A. (2014). Modify or die?--RNA modification defects in metazoans. RNA Biol *11*, 1555-1567.

Saxton, R.A., and Sabatini, D.M. (2017). mTOR Signaling in Growth, Metabolism, and Disease. Cell *168*, 960-976.

Schaechter, M., Maaloe, O., and Kjeldgaard, N.O. (1958). Dependency on medium and temperature of cell size and chemical composition during balanced grown of Salmonella typhimurium. J Gen Microbiol *19*, 592-606.

Schirmaier, F., and Philippsen, P. (1984). Identification of two genes coding for the translation elongation factor EF-1 alpha of S. cerevisiae. EMBO J *3*, 3311-3315.

Schito, L., and Semenza, G.L. (2016). Hypoxia-Inducible Factors: Master Regulators of Cancer Progression. Trends Cancer *2*, 758-770.

Schwartz, S., Bernstein, D.A., Mumbach, M.R., Jovanovic, M., Herbst, R.H., Leon-Ricardo, B.X., Engreitz, J.M., Guttman, M., Satija, R., Lander, E.S.*, et al.* (2014). Transcriptome-wide mapping reveals widespread dynamic-regulated pseudouridylation of ncRNA and mRNA. Cell *159*, 148-162.

Sharon, E., Chen, S.A., Khosla, N.M., Smith, J.D., Pritchard, J.K., and Fraser, H.B. (2018). Functional Genetic Variants Revealed by Massively Parallel Precise Genome Editing. Cell *175*, 544-557 e516.

She, R., and Jarosz, D.F. (2018). Mapping Causal Variants with Single-Nucleotide Resolution Reveals Biochemical Drivers of Phenotypic Change. Cell *172*, 478-490 e415.

Shorter, J., and Lindquist, S. (2004). Hsp104 catalyzes formation and elimination of self-replicating Sup35 prion conformers. Science *304*, 1793-1797.

Shorter, J., and Lindquist, S. (2005). Prions as adaptive conduits of memory and inheritance. Nat Rev Genet *6*, 435-450.

Singh, A., Helms, C., and Sherman, F. (1979). Mutation of the non-Mendelian suppressor, Psi, in yeast by hypertonic media. Proc Natl Acad Sci U S A *76*, 1952-1956.

Sonenberg, N. (1993). Translation factors as effectors of cell growth and tumorigenesis. Curr Opin Cell Biol *5*, 955-960.

1727 Sonenberg, N., and Hinnebusch, A.G. (2009). Regulation of translation initiation in
1728 eukaryotes: mechanisms and biological targets. Cell *136*, 731-745.

1729 Steffen, K.K., and Dillin, A. (2016). A Ribosomal Perspective on Proteostasis and Aging.
1730 Cell Metab *23*, 1004-1012.

1731 Steffen, K.K., Kennedy, B.K., and Kaeberlein, M. (2009). Measuring replicative life span
1732 in the budding yeast. J Vis Exp.

1733 Storici, F., and Resnick, M.A. (2006). The delitto perfetto approach to in vivo site-
1734 directed mutagenesis and chromosome rearrangements with synthetic oligonucleotides
1735 in yeast. Methods Enzymol *409*, 329-345.

1736 Su, T.T., and O'Farrell, P.H. (1998). Size control: cell proliferation does not equal
1737 growth. Curr Biol *8*, R687-689.

1738 Suzuki, G., Shimazu, N., and Tanaka, M. (2012). A yeast prion, Mod5, promotes
1739 acquired drug resistance and cell survival under environmental stress. Science *336*,
1740 355-359.

1741 Tanenbaum, M.E., Stern-Ginossar, N., Weissman, J.S., and Vale, R.D. (2015).
1742 Regulation of mRNA translation during mitosis. Elife *4*.

1743 Terada, N., Patel, H.R., Takase, K., Kohno, K., Nairn, A.C., and Gelfand, E.W. (1994).
1744 Rapamycin selectively inhibits translation of mRNAs encoding elongation factors and
1745 ribosomal proteins. Proc Natl Acad Sci U S A *91*, 11477-11481.

1746 Tuite, M.F., Mundy, C.R., and Cox, B.S. (1981). Agents that cause a high frequency of
1747 genetic change from [psi+] to [psi-] in Saccharomyces cerevisiae. Genetics *98*, 691-711.

1748 Tuller, T., Carmi, A., Vestsigian, K., Navon, S., Dorfan, Y., Zaborske, J., Pan, T., Dahan,
1749 O., Furman, I., and Pilpel, Y. (2010). An evolutionarily conserved mechanism for
1750 controlling the efficiency of protein translation. Cell *141*, 344-354.

1751 Turner, J.J., Ewald, J.C., and Skotheim, J.M. (2012). Cell size control in yeast. Curr Biol
1752 *22*, R350-359.

1753 Urban, J., Soulard, A., Huber, A., Lippman, S., Mukhopadhyay, D., Deloche, O., Wanke,
1754 V., Anrather, D., Ammerer, G., Riezman, H.*, et al.* (2007). Sch9 is a major target of
1755 TORC1 in Saccharomyces cerevisiae. Mol Cell *26*, 663-674.

1756 Vallen, E.A., Hiller, M.A., Scherson, T.Y., and Rose, M.D. (1992). Separate domains of
1757 KAR1 mediate distinct functions in mitosis and nuclear fusion. J Cell Biol *117*, 1277-
1758 1287.

1759 Varlakhanova, N.V., Tornabene, B.A., and Ford, M.G.J. (2018). Feedback regulation of
1760 TORC1 by its downstream effectors Npr1 and Par32. Mol Biol Cell *29*, 2751-2765.

1761 Wang, M., Liu, H., Zheng, J., Chen, B., Zhou, M., Fan, W., Wang, H., Liang, X., Zhou,
1762 X., Eriani, G.*, et al.* (2016). A Deafness- and Diabetes-associated tRNA Mutation
1763 Causes Deficient Pseudouridinylation at Position 55 in tRNAGlu and Mitochondrial
1764 Dysfunction. J Biol Chem *291*, 21029-21041.

1765 Warner, J.R., and Knopf, P.M. (2002). The discovery of polyribosomes. Trends in
1766 biochemical sciences *27*, 376-380.

1767 Wasko, B.M., Carr, D.T., Tung, H., Doan, H., Schurman, N., Neault, J.R., Feng, J., Lee,
1768 J., Zipkin, B., Mouser, J.*, et al.* (2013). Buffering the pH of the culture medium does not
1769 extend yeast replicative lifespan. F1000Res *2*, 216.

1770 Weill, U., Yofe, I., Sass, E., Stynen, B., Davidi, D., Natarajan, J., Ben-Menachem, R.,
1771 Avihou, Z., Goldman, O., Harpaz, N.*, et al.* (2018). Genome-wide SWAp-Tag yeast
1772 libraries for proteome exploration. Nat Methods *15*, 617-622.

1773 Werner-Washburne, M., Becker, J., Kosic-Smithers, J., and Craig, E.A. (1989). Yeast
1774 Hsp70 RNA levels vary in response to the physiological status of the cell. J Bacteriol
1775 *171*, 2680-2688.

1776 Werner-Washburne, M., and Craig, E.A. (1989). Expression of members of the
1777 Saccharomyces cerevisiae hsp70 multigene family. Genome *31*, 684-689.

1778 Wickner, R.B. (1994). [URE3] as an altered URE2 protein: evidence for a prion analog
1779 in Saccharomyces cerevisiae. Science *264*, 566-569.

1780 Wickner, R.B. (2016). Yeast and Fungal Prions. Cold Spring Harb Perspect Biol *8*.

1781 Yang, J., Dungrawala, H., Hua, H., Manukyan, A., Abraham, L., Lane, W., Mead, H.,
1782 Wright, J., and Schneider, B.L. (2011). Cell size and growth rate are major determinants
1783 of replicative lifespan. Cell Cycle *10*, 144-155.

1784 Yofe, I., Weill, U., Meurer, M., Chuartzman, S., Zalckvar, E., Goldman, O., Ben-Dor, S.,
1785 Schutze, C., Wiedemann, N., Knop, M.*, et al.* (2016). One library to make them all:
1786 streamlining the creation of yeast libraries via a SWAp-Tag strategy. Nat Methods *13*,
1787 371-378.

1788 Yuan, A.H., and Hochschild, A. (2017). A bacterial global regulator forms a prion.
1789 Science *355*, 198-201.

1790 Zadrag-Tecza, R., Kwolek-Mirek, M., Bartosz, G., and Bilinski, T. (2009). Cell volume as
1791 a factor limiting the replicative lifespan of the yeast Saccharomyces cerevisiae.
1792 Biogerontology *10*, 481-488.

1793 Zaringhalam, M., and Papavasiliou, F.N. (2016). Pseudouridylation meets next-
1794 generation sequencing. Methods *107*, 63-72.

Zhang, H., Stallock, J.P., Ng, J.C., Reinhard, C., and Neufeld, T.P. (2000). Regulation of cellular growth by the Drosophila target of rapamycin dTOR. Genes Dev *14*, 2712-2724.

Zhao, B.S., Roundtree, I.A., and He, C. (2017). Post-transcriptional gene regulation by mRNA modifications. Nat Rev Mol Cell Biol *18*, 31-42.

Zucchini, C., Strippoli, P., Biolchi, A., Solmi, R., Lenzi, L., D'Addabbo, P., Carinci, P., and Valvassori, L. (2003). The human TruB family of pseudouridine synthase genes, including the Dyskeratosis Congenita 1 gene and the novel member TRUB1. Int J Mol Med *11*, 697-704.